Biosonar Responsivity Sets the Stage for the Terminal Buzz

Ravi Umadi[1] Uwe Firzlaff[1]

[1] Lehrstuhl für Zoologie, TUM School of Life Sciences, Technische Universität München, Liesel-Beckmann-Str. 4, 85354, Freising-Weihenstephan, Germany

Abstract. Echolocating bats dynamically adjust their sonar signals during prey pursuit, yet the mechanistic limits that govern these rapid transitions have remained unclear. Here, we introduce the *responsivity framework*, a predictive model that formalises the scaling between echo delay, call rate, and relative velocity through a single parameter–the responsivity coefficient k_r. From this relation, we derive biologically interpretable quantities such as the reaction window T_b and the *buzz-readiness threshold*, marking the onset of a high-gain sensorimotor regime preceding the terminal buzz.

Simulations of bat–prey interactions, incorporating both stationary and motile targets, reproduced systematic velocity–call-rate trade-offs and realistic behavioural profiles, from which distances, velocities, and reaction times could be inferred using call timing alone. Internal consistency checks confirmed that the framework's analytical identities for distance and velocity hold across sequences, while spatio–temporal maps revealed how T_b contracts with increasing k_r and velocity, defining the biophysical limit of temporal control. Comparisons with high-resolution field recordings showed that observed call-rate dynamics followed the predicted trends, with variability arising from environmental context and localisation uncertainty.

By linking simple acoustic observables to a broad set of derived parameters, the responsivity framework provides a *mechanistic and predictive tool* for interpreting echolocation behaviour. It explains variable buzz lengths and reaction limits consistent with experimental observations. It establishes a general principle: sequential adaptive behaviours unfold under constraints set by the *speed of regulatory feedback*. While demonstrated in bat biosonar, this principle offers broader relevance to understanding adaptive control and sensory–motor integration across biological systems.

Keywords: Echolocation, Responsivity framework, Call rate adaptation, Reaction window, Buzz readiness, Velocity–call rate tradeoff, Sensorimotor control, Feedback loops, Prey interception, Adaptive behaviour

1 INTRODUCTION

Echolocating bats exemplify the sophistication of active sensory systems, where the dynamic and rapid behavioural adaptations have long been recognised as central to navigating the environment and intercepting prey [1–4]. An echolocating bat emits short, high-frequency calls, listens to the echoes to obtain information about its surroundings, and adjusts the call and behavioural parameters as necessary. When a target is detected, the bat approaches it and transitions into

Corresponding author: Ravi Umadi– Email: ravi.umadi@tum.de

shorter and more frequent calls. A successful interception is assumed to be characterised by a rapid succession of calls at up to 200 calls per second at the end—a phenomenon known as *terminal buzz*. Field and laboratory studies have established that the echolocating bat modulates every parameter of the acoustic response as the context demands [5–9]. A key insight from studies of other predator–prey systems is the importance of speed and reaction time in successful hunting. This has been well characterised in cursorial predators like cheetahs chasing antelopes [10]. However, it remains underexplored in volant predators such as bats. Other than the crucial calling frequency adaptations in response to the Doppler effect in constant frequency call emitters [11–15], this fundamental physical parameter has received comparatively little attention.

Recent work by Jakobsen et al. (2025) [16] demonstrated that echolocation behaviour in aerial-hawking bats is more closely regulated by flight velocity than by absolute prey distance. Their findings underscore the role of temporal parameters in shaping kinematic decision-making, suggesting that precise call timing is central to sensory-motor coordination. However, while the study elevates the importance of velocity in echolocation control, it stops short of providing a mechanistic or predictive framework for how velocity drives adaptations in sonar behaviour during interception tasks.

As extensive as echolocation research has been over the decades, a generalised mathematical model and predictive framework have remained elusive.

The pace at which predator-prey interactions play out further compels understanding of the time sequence of actions and events in a racing system of rapid sensory-motor calibrations with evolving strategies. The time beacons of the echolocation calls make the system particularly amenable to temporal delineation, with which the limits of the system parameters may be revealed.

One such characterisation is the rate at which the changing parameters adapt to demanding contexts, a function we introduce as *responsivity*, which we incorporate in a mathematical framework that formalises the relationship between call rate, echo delay, relative velocity, and use it to deduce the limit of the biological reaction time of the echolocating animals. By treating sonar responsivity as a measurable function of the temporal dynamics between call emission and echo arrival, we derive a novel limit - termed *buzz readiness* - beyond which further increases to call rate adaptations offer no additional sensory-motor advantage.

The central hypothesis of this study is that the relative velocity between the bat and its target governs the emergence of interception strategies via a tradeoff between speed and sonar update rate. At higher relative velocities, the system reaches its reaction threshold closer to the target, often constraining or eliminating the production of a long terminal buzz. The responsivity is primed earlier at lower velocities, permitting extended call rate acceleration and facilitating a full buzz. This tradeoff predicts behavioural outcomes, such as capture success or abandonment, and reveals how echolocation call dynamics are tuned to optimise sensory acquisition within a velocity-bounded temporal envelope.

To validate the insights provided by this framework, we developed a simulated echolocation system that mimics the real-world phenomenon and offers the advantage of tuning behavioural parameters to study the outcomes. Further, we recorded foraging wild bats with a microphone array and calculated acoustic, kinetic and behavioural parameters to verify the hypotheses. Our results proved the theoretical framework and show that the interception strategies evolve due to the velocity-call rate tradeoff, where the innate biological limits play a central role.

In this study, we formalise sonar responsivity as a predictive and mechanistic framework for echolocation behaviour, primarily focused on frequency-modulated (FM) call emitters. The framework builds on a key insight: *the pace of adaptive behavioural changes, when unfolding in real time, is constrained by the speed of the regulatory feedback that governs them.* Applied to bat sonar, the round-trip propagation delay bounds call rate acceleration and the neural feedback loop, formalised through a single scaling coefficient k_r. From this scaling relation, the framework yields a set of derivable parameters, including the reaction window T_b, the prime responsivity point $\mathcal{R}^*$ or buzz readiness, that define the temporal limits of sonar-guided pursuit. The simulation outputs reproduced known features of bat call dynamics and provided internally consistent identities for velocity and distance. At the same time, field recordings revealed behavioural profiles that broadly conformed to the predicted tradeoff between call rate and relative velocity, albeit with greater variability due to localisation noise and environmental context.

These results show that the responsivity framework offers more than a descriptive account of buzz behaviour: it provides an analytical tool for inferring otherwise inaccessible parameters, such as target distance, approach velocity, and reaction thresholds, from simple call recordings. By situating echolocation dynamics within a principled scaling law, this work advances a general theory of how sensorimotor constraints shape interception strategies in volant predators and establishes a foundation for extending these insights across species, call types, and other active sensory systems.

2 METHODS

Echolocation is an *active sensory system*, in which perception is not passively received but actively generated and updated through call production. Each call triggers echoes that must be processed before the next call is emitted, embedding a strict temporal coupling between sensory input and motor output. The efficiency of this loop depends not only on how fast calls are produced, but also on how flexibly and finely their timing can be adjusted as conditions change.

We describe this adaptive capacity with the term *Responsivity*. Etymologically, the word stems from the Latin *respondere* ("to answer, to respond"), highlighting its role as a measure of how dynamically the sonar system "answers back" to shifting sensory demands. In this framework, responsivity refers to the sensitivity of adjustment rather than absolute speed: it captures how delicately interpulse intervals are tuned when approaching a target, when echo–call overlap looms, or when a bat must increase its update rate to maintain accurate tracking.

By focusing on responsivity, we aim to quantify a property of echolocation that bridges behaviour and physiology: the bat's ability to translate sensory feedback into precisely scaled changes in call timing. This conceptual definition provides the foundation for its mathematical formulation in the following subsection.

2.1 The Responsivity Framework

The responsivity metric $\mathcal{R}$, defined as the inverse of the change in interpulse interval (IPI), captures more than just the magnitude of temporal adaptation; it quantifies the echolocation system's capacity for fine motor control under increasing sensory demands. As the bat approaches a target, its IPIs shrink progressively, reflecting a rising need to update sonar information more frequently. Although $\mathcal{R}$ peaks when the call rate is the highest, its inflexion point occurs when

the bat begins to make the *smallest possible adjustments* in IPI to continue adapting its call rate. In this regime, even minute changes in IPI reflect substantial control effort–the finer control and coordination efforts being more demanding than coarser control efforts [17, 18]. Thus, $\mathcal{R}$ is not a measure of speed, but of sensitivity – how delicately the bat can tune its sonar output in response to a rapidly evolving scene.

This behaviour is analogous to fine motor control in other biological systems. When the system begins operating near its physiological limits, it must exert greater control to maintain stability and precision. A high value of $\mathcal{R}$ implies that the bat is entering a state where temporal motor control is maximally engaged - where the *ability* to make small changes in timing becomes crucial to avoiding echo-call overlap, maintaining sensory coherence, and preparing for the imminent need to emit pulses at the maximum call rate. Therefore, we interpret that transition point in $\mathcal{R}$ as the onset of *buzz readiness*: the point at which the bat's sonar system is fully mobilised to deliver its fastest, most focused interrogation of the environment. The maximum call rate defines this threshold, but in terms of the ability to make the smallest changes required to achieve that rate – an anticipatory signal that the terminal buzz is near (See the mathematical definition in Section 2.1.2.).

2.1.1 Call Events and Responsivity Coefficient k_r

To estimate the theoretical lower bounds of biological reaction time in echolocating bats, we modelled the timing dynamics between emitted calls and their returning echoes as a function of target distance and sound propagation (see figure 1a). The acoustic travel time, denoted as T_a, was defined as the two-way delay between a call emission and its echo return, accounting for the bat's own displacement during this interval:

$$T_a = \frac{2d(t) - \Delta s}{c} \tag{1}$$

Where $d(t)$ is the instantaneous distance to the target, Δs is the displacement of the bat during sound travel, and c is the speed of sound in air. The total interval between two call emissions Δt (IPI) is composed of T_a and the bat's biological reaction time window T_b, modeled as a proportional function of T_a:

$$T_b = k_r \cdot T_a \tag{2}$$

And,

$$\Delta t = T_a + T_b \tag{3}$$

Here, k_r is a dimensionless biological reaction constant that scales the available reaction time window with respect to echo delay. It corresponds to the entire sensory-motor processing time, from echo reception to subsequent call emission. The call rate C_r is then calculated as the inverse of the total interval:

$$C_r = \frac{1}{\Delta t} = \frac{1}{T_a(1 + k_r)} \tag{4}$$

2.1.2 Responsivity Thresholds

To quantify the temporal sharpness of adaptation during echolocation, we define a metric called *responsivity*, which reflects the bat's capacity to make precise, moment-to-moment changes in

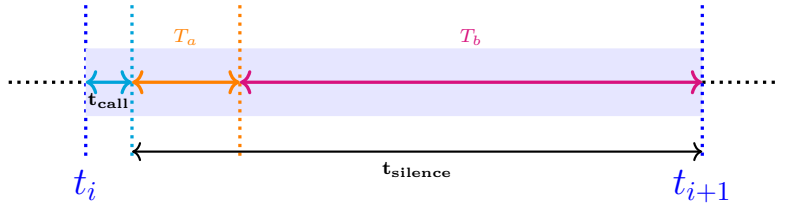

(a) Call Event Model

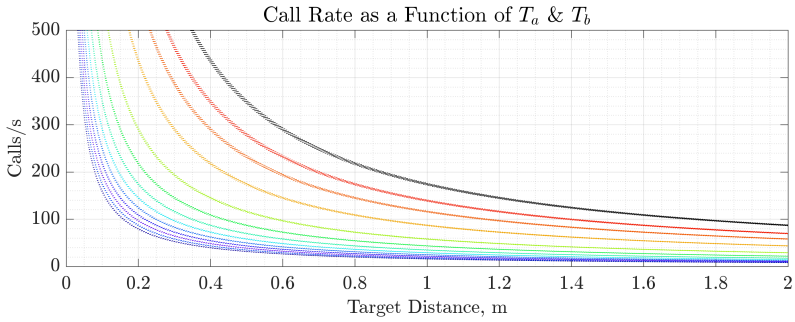

(b) Call Rate Limit At Decreasing Target Distances

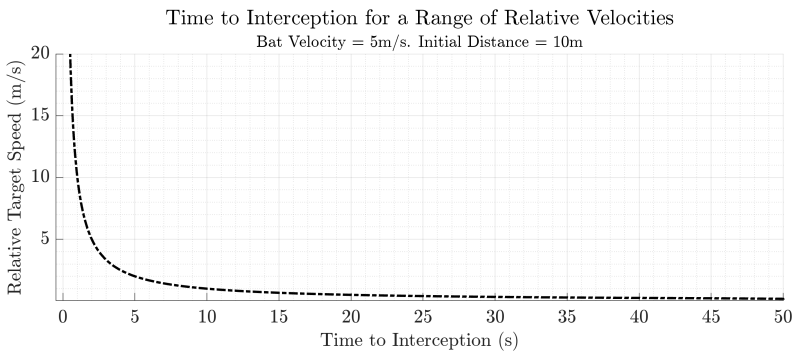

(c) Time to Interception

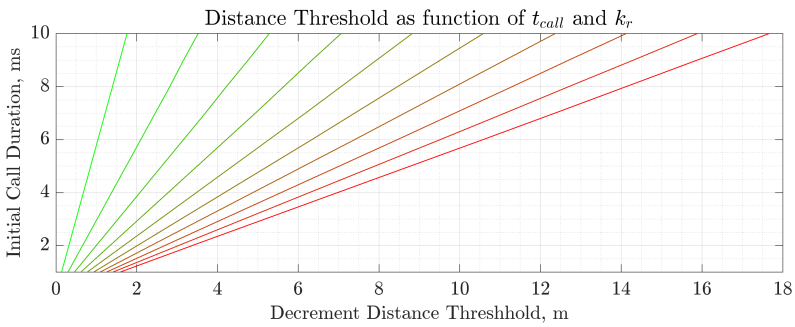

(d) Call Duration Decrement Model

Figure 1: Temporal parameters and limits. (**a**) Schematic of the call event model, showing the temporal sequence of emission (t_i), echo return (T_a), and processing–response window (T_b). As the bat approaches a target, the acoustic travel time T_a shortens and the available processing interval T_b decreases accordingly, thereby defining the temporal limit at which successive calls can be emitted. The call sequence may thus be expressed as $[t_i, t_{i+1} ... t_N] = \bigcup_{n=1}^{N} [T_a, T_p, T_r, T_l]^n$, where processing ($T_p$) and response ($T_r$) components sum to T_b, and lag (T_l) is assumed negligible or absent. (**b**) Relationship between call rate and target distance derived from the responsivity framework. The model defines call rate as $r_c = 1/(T_a + T_b)$, where $T_b = k_r T_a$. Varying k_r (0, 0.25, 0.5, 1, 2 ...10; black to dark blue) produces distinct scaling curves, showing that call rate increases nonlinearly as distance decreases. The curvature of these functions allows k_r to be empirically approximated from measured call rate–distance data. (**c**) Time-to-interception as a function of relative velocity, showing the rapid nonlinear decay of interception time as relative velocity increases. (**d**) Call duration decrement model illustrating, for a given initial call duration, the distance at which $t_{\text{call}} \approx T_a + T_{b^*}$. Curves are colour-coded for k_r = 1–10 (green to red) at 5 m/s, showing how increasing responsivity (i.e., lower K_r) compresses the range over which call shortening occurs.

its interpulse interval (IPI) as target distance decreases. This measure captures how rapidly the bat is increasing its call rate, and how *finely* it can adjust sonar timing in anticipation of the terminal buzz.

The IPI at call index n is,

$$\Delta t_n = t_{n+1} - t_n, \tag{5}$$

where t_n is the timestamp of the n-th call. Responsivity at index n (*instantaneous responsivity*) is then expressed as the inverse of the change in IPI magnitude between successive calls:

$$\mathcal{R}_n = \left| \frac{1}{(\Delta t_{n+1} - \Delta t_n)} \right| \tag{6}$$

High values of $\mathcal{R}_n$ occur when the sonar system makes extremely small timing adjustments, indicative of maximal fine-grained temporal control. This regime enables the bat to avoid sensory interference (e.g. echo–call overlap, managed by call duration contraction) and to approach its maximum call rate without overshooting it.

Anchoring to $C_{r,\max}$. We anchor the identification of prime responsivity to the species-specific maximum call rate $C_{r,\max}$, providing a physiologically meaningful temporal control ceiling. $C_{r,\max}$ reflects the shortest feasible loop time of the sonar system—the sum of the minimal echo delay and minimal sensorimotor processing time—and thus embodies the ultimate constraint on how fast the bat can operate. Near this ceiling, absolute increases in call rate are limited, but the bat must still make progressively smaller adjustments to avoid surpassing its physiological bounds. Responsivity therefore begins to saturate in this regime, and linking $\mathcal{R}$ to $C_{r,\max}$ ensures that the metric reflects control effort rather than incidental fluctuations earlier in the approach.

Buzz readiness point. To locate the onset of this transition, we compute $\mathcal{R}_n$ across the call sequence as a *responsivity curve* and identify the index n^* within the ceiling neighbourhood where responsivity is approaching inflexion. Because $\mathcal{R}_n$ and call rate C_r share identical physical units (s^{-1}), responsivity can be expressed in dimensionless form by normalising to the physiological ceiling $C_{r,\max}$:

$$\tilde{\mathcal{R}}_n = \frac{\mathcal{R}_n}{C_{r,\max}}. \tag{7}$$

At the condition $\tilde{\mathcal{R}}_n \approx 1$, the rate of temporal adjustment approaches the highest attainable sensory update rate, marking the point where the sonar loop begins to operate at its maximal effective gain. This state, denoted as *prime responsivity* ($\mathcal{R}^*$), corresponds to the inflexion point of the control curve where further increases in call rate yield diminishing adaptive returns.

Operationally, we determine this point by anchoring to the physiological ceiling $C_{r,\max}$ and identifying the *inflexion index* that minimises the difference between responsivity and call rate,

$$n^* = \arg\min_n \left| \mathcal{R}_n - C_{r_{\max}} \right|. \tag{8}$$

This index n^* marks the *buzz readiness point*—the call at which the sonar control system transitions into its maximum-gain regime, fully primed for terminal tracking. By defining buzz readiness in terms of $\tilde{\mathcal{R}}_n$, the framework provides an objective and reproducible threshold that

reflects the intrinsic dynamics of sensorimotor regulation, rather than an arbitrarily imposed call rate boundary.

Reaction time threshold. At n^*, we define the *reaction time threshold* T_{b^*} as the absolute inter-pulse interval (IPI) change realised at the point of buzz readiness:

$$T_{b^*} = \left|\Delta t_{n^*+1} - \Delta t_{n^*}\right| \tag{9}$$

Physiologically, T_{b^*} represents the minimal temporal step the sonar control loop can accommodate while approaching $C_{r,\max}$. A small T_{b^*} indicates rapid, fine-scale acceleration into the buzz, whereas a larger value reflects a more gradual transition. While T_{b^*} corresponds conceptually to behavioural reaction time limits observed in prey-removal experiments [6], it remains a *model-derived* quantity. Further experimental validation is needed to determine how closely T_{b^*} maps onto physiological latencies of neural processing and motor execution in freely behaving bats.

Interpretation. The pair $(\mathcal{R}^*, T_{b^*})$ thus characterises the bat's sensorimotor posture at the threshold of the buzz: $\mathcal{R}^*$ quantifies the intensity of fine-tuned temporal control, and T_{b^*} quantifies the minimal actionable increment available to the sonar loop. Because these values are anchored to $C_{r,\max}$, they provide a generalisable, physiology-linked descriptor of buzz readiness that can be applied across species and conditions. Importantly, this method does not depend on absolute IPI or call rate values, but on their pattern of change, making it robust to inter-individual and interspecific variation, provided a reasonable estimate of $C_{r,\max}$ is available.

2.2 Simulation of Predator-Prey Dynamics

2.2.1 Simulator Implementation

To simulate the temporal structure of echolocation calls during an approach sequence, we implemented a custom function `simulateEcholocation()` in MATLAB, which generates synthetic call–echo interactions under the responsivity framework. The simulator models the interplay between acoustic travel time, call timing, and target motion, while providing flexible options to include stochasticity in target movement and synthetic audio rendering. This section summarises the high-level structure of the simulation. The technical implementations are discussed in the following sections.

```
result = simulateEcholocation(bandwidth, kr, ...
target_distance, ...
initial_velocity, ...
initial_call_duration, ...
motile, makeAudio)
```

Listing 1: Function signature and inputs of `simulateEcholocation`.

Inputs:

- `bandwidth` [Hz] 1×2 vector specifying call frequency range
- `kr` [–] responsivity coefficient scaling echo delay into inter-pulse interval (IPI)
- `target_distance` [m] initial range to the target

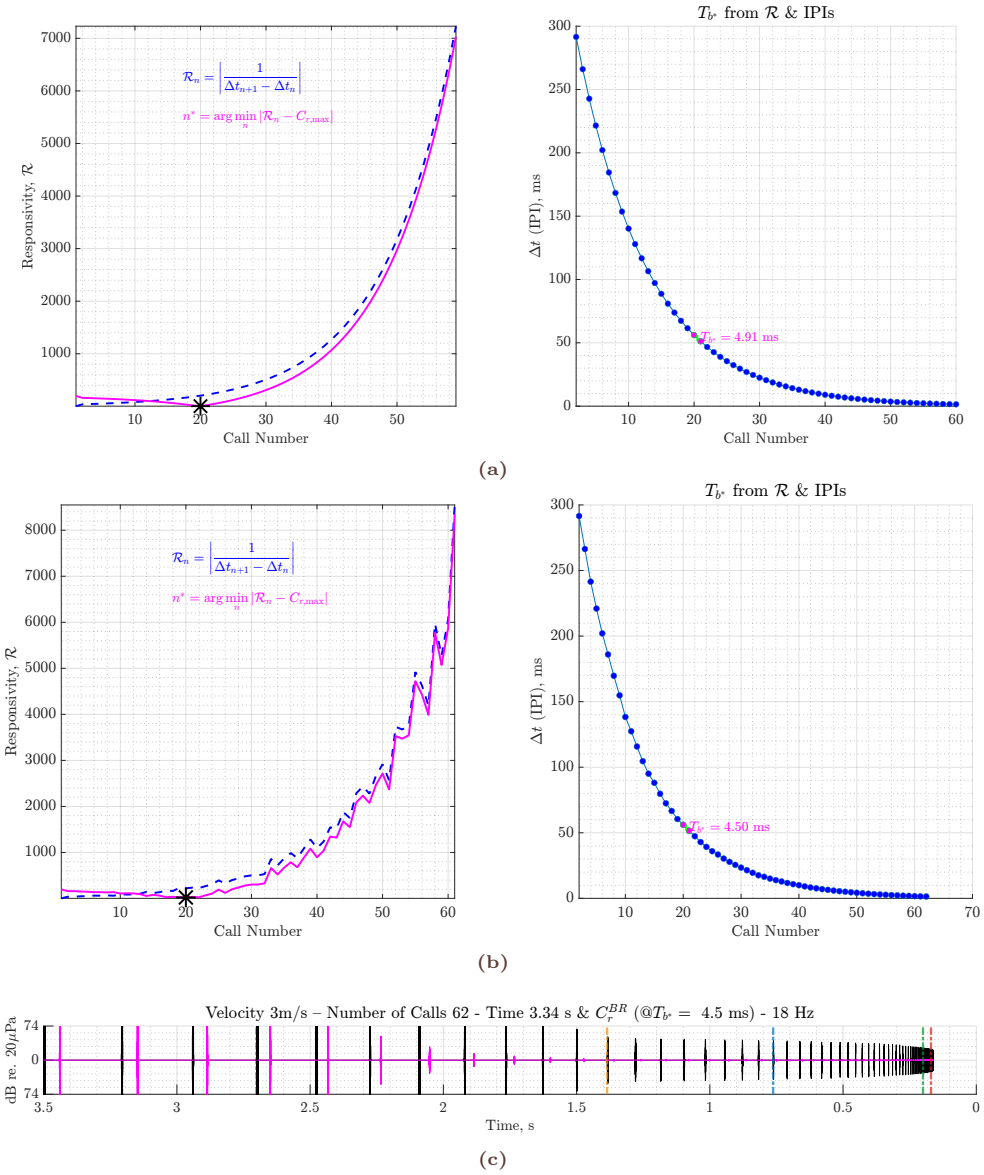

Figure 2: Deriving responsivity $\mathcal{R}_n$ and the buzz readiness time T_{b^*}. (**a**) Stationary prey simulation at $v_{init} = 3$ m/s and $d = 10$ m. (**b**) Motile prey simulation with a 10% stochastic tracking inaccuracy in prey position, scaled with relative velocity at each step, thereby mimicking natural variability from random prey motion and biomechanical constraints. In both cases, the inflexion point (minimum of the magenta curve) indicates prime responsivity, marking the buzz readiness threshold. This point (black asterisk) reflects when the bat must begin exerting its finest control to maintain sonar adaptability without exceeding physiological constraints. In real-world pursuits, bats may transiently approach this state multiple times depending on echo delays and environmental complexity (e.g., clutter or obstacles). (**c**) Call–echo sequence (black and magenta, respectively) from the motile simulation, showing annotated events: call duration decrement (orange), buzz readiness (blue), buzz point (green), and call–echo overlap (red). The call rate at buzz readiness, and thus the reaction time threshold, depends on relative velocity (see Figure 7).

- `initial_velocity` [m/s] approach velocity toward the target
- `initial_call_duration` [s] starting duration of emitted calls
- `motile` [logical] include stochastic target motion if true
- `makeAudio` [logical] synthesise audio waveforms if true

Outputs: The function returns a structured array containing kinematic, acoustic, and timing variables for the full approach sequence:

```
result.delta_s                % stepwise distance changes between calls
result.delta_t                % inter-pulse intervals (IPI)
result.call_rate_responsivity% instantaneous responsivity (Hz)
result.call_levels            % call amplitudes
result.call_points            % call timestamps (sample indices)
result.decrement_point        % index where call duration starts decreasing
result.detection_point        % index where echo detection crosses threshold
result.echo_points            % echo return timestamps (sample indices)
result.echo_time              % time of each echo arrival (s) - for audio generation
result.initial_velocity       % input parameter, starting velocity of bat
result.new_amplitude          % updated amplitude per call
result.new_call_duration      % updated call duration array
result.initial_target_distance % input parameter
result.new_target_distance    % updated target distance after each call
result.Ta                     % two-way travel time per call (s)
result.Tb                     % biological reaction window
result.Tb_prime               % reaction time threshold
result.Tb_idx                 % index corresponding to Tb* and R*
result.time_to_contact        % estimated remaining time to reach target
result.TS                     % target strength per call
result.Kr                     % input responsivity coefficient
result.max_call_rate          % max physiologically plausible call rate (Hz), empirical/assumed value
result.MaxCallRatePoint       % index when IPI reaches max rate
result.OverlapPoint           % index where call-echo overlap starts
result.audio                  % 2-column [call, echo] waveform if makeAudio=true
```

Listing 2: Complete list of output fields returned by `simulateEcholocation`.

Overview of method: At each simulation step, the instantaneous target distance defines the acoustic two-way delay T_a, which is scaled by the responsivity factor k_r to determine the subsequent inter-pulse interval $\Delta t = T_a + T_b$. The model updates the bat–target distance by integrating forward displacement, optionally perturbed by noise when `motile` is enabled. Call durations are adapted in relation to T_a, while amplitude is updated based on propagation loss and detection thresholds.

When `makeAudio` is true, each call is synthesised within the specified frequency band, convolved with air attenuation filters, and paired with its echo at the appropriate delay. The FM call generation procedure follows the approach described in our previous work on microphone array design and spatial tracking accuracy simulations [19, 20].

This modular structure allows simulation of approach sequences under the responsivity framework. It provides outputs that can be directly cross-validated against analytical predictions of distance, velocity, and call rate dynamics.

2.2.2 Target Update and Predator-Prey Dynamics with Noise

At each echolocation event, the bat's forward displacement is computed as

$$\Delta s(n) = v_{\text{bat}} \cdot \Delta t(n+1) \tag{10}$$

and subtracted from the previous target range:

$$d(n+1) = d(n) - \Delta s(n) \tag{11}$$

This iterative update continues until the target distance becomes zero or negative, indicating interception.

We extended this deterministic update by incorporating stochastic variability to mimic biologically realistic pursuit behaviour. The change in target distance per step was defined as

$$\Delta s_n = v_0 \cdot \Delta t_{n+1} + \epsilon_n, \tag{12}$$

where v_0 is the initial relative velocity and ϵ_n is a Gaussian noise term capturing stochastic tracking errors by the bat, or random prey displacement. To ensure proportional scaling, noise was added relative to the expected step size:

$$\epsilon_n = k_{\text{noise}} \cdot v_0 \cdot \Delta t_{n+1} \cdot \eta_n, \qquad \eta_n \sim \mathcal{N}(0,1) \tag{13}$$

In the runs simulating motile prey, a random jitter ($k_{noise} = 0.1$) was added to Δs_n, representing variable relative motion of the target (see Figures 2b & 2c).

The call rate per step was calculated as

$$C_r = \min\left(\frac{1}{\Delta t}, C_{r,\max}\right)$$

with an upper ceiling $C_{r,\max} = 200\,\text{Hz}$ to mimic the terminal buzz constraint.

To quantify the scaling relationship between relative velocity (v_r) and call rate (C_r), we fitted a power-law model of the form,

$$v_r = K\, C_r^b$$

Uncertainty in the fitted parameters was assessed using non-parametric bootstrapping: we resampled the (C_r, v_r) pairs with replacement $N = 10^4$ times, refitted the power-law on each bootstrap replicate, and extracted the 2.5^{th} and 97.5^{th} percentiles of the parameter distributions. This yielded bias-corrected 95% confidence intervals for the scaling exponent b and prefactor K, ensuring robust comparison between simulation and field data.

2.2.3 Echo Level and Detectability

For each echolocation event, the simulation models the received level of the echo signal based on the bat's distance to the target and the acoustic environment. The target strength $TS(n)$ is computed as a function of the call frequency, the target's effective diameter, and the distance at

the $(n+1)$-th call, incorporating frequency-dependent atmospheric attenuation $\alpha(f, T, RH, P)$:

$$TS(n) = f_{\text{TS}}\left(f_{\text{min}}, D_{\text{target}}, d(n+1), \alpha\right) \tag{14}$$

To account for signal loss during propagation, the model includes geometric spreading attenuation $TL(n)$, calculated as a round-trip loss:

$$TL(n) = 2 \cdot f_{\text{geom_atten}}(d(n+1)) \tag{15}$$

The received level $RL(n)$ at the bat's ears is then given by:

$$RL(n) = SL - |TL(n)| + TS(n) \tag{16}$$

where SL is the emitted source level. The echo is considered undetectable if the received level falls below a defined detection threshold. This threshold condition enables the simulation to determine the point of target detectability during the approach. These calculations allow the system to dynamically assess whether each returning echo is strong enough to inform further motor actions or call adjustments.

2.2.4 Call Duration Contraction Threshold

As the bat approaches its target, the acoustic travel time (T_a) between call emission and echo reception decreases. To avoid overlap between outgoing calls and returning echoes, the bat must reduce the duration of its calls in accordance with the shrinking echo delay. This necessity defines a threshold for call duration contraction, governed by the inequality:

$$t_{\text{call}} < T_a + T_{b^*} \tag{17}$$

where t_{call} is the emitted call duration. The distance at which this inequality becomes critical can be used to estimate the spatial onset of call duration decrement.

To determine this distance threshold, the inequality can be rearranged as:

$$d_c = \frac{t_{\text{call}} \cdot c}{2} + T_{b^*} \cdot v \tag{18}$$

where d_c is the critical distance at which call duration contraction must begin, and v is the bat's relative velocity. Figure 1d illustrates how this threshold varies for different values of the reaction constant k_r, which modulates T_b as a multiple of T_a.

In the simulation, the bat reduces its call duration when the current target distance $d(t)$ falls below the calculated contraction threshold. This dynamic ensures that emitted calls do not interfere with echo processing, especially during the final phases of the approach. The onset of call duration contraction, when mapped alongside the moment of target detection and the point of prime responsivity, provides insight into how bats temporally coordinate their vocal and perceptual systems for successful interception (See Figure 7).

2.2.5 Call Duration Adjustment with Stochastic Perturbation

In addition to modelling the distance dynamics and call timing, we incorporated a biologically plausible adjustment of call duration across successive calls. At the onset of the decrement phase

(index $n = n_{\text{dec}}$), the call duration t_n was reduced in proportion to the echo delay T_a, scaled by the responsivity coefficient k_r:

$$t_n = \begin{cases} t_0, & n < n_{\text{dec}}, \\ \max\left(\frac{T_{a,n}}{k_r}, t_{\min}\right), & n \geq n_{\text{dec}}, \end{cases}$$

where t_0 is the initial call duration, $t_{\min} = 0.5\,\text{ms}$ represents the lower physiological bound, and $T_{a,n}$ is the echo delay at step n.

To avoid perfectly deterministic trajectories and reflect observed biological variability, we further added a Gaussian perturbation to each call duration:

$$t_n \leftarrow \min\Big(t_0,\ t_n + \sigma_t\,\eta_n\Big), \qquad \eta_n \sim \mathcal{N}(0,1),$$

with $\sigma_t = 0.4\,\text{ms}$ representing the standard deviation of the stochastic adjustment. This ensures that call durations fluctuate around the deterministic trajectory, while remaining bounded between $t_{\min}$ and the initial value t_0.

This stochastic refinement prevents artificial alignment artefacts in the simulated data and more closely mimics the natural variability of call duration adjustments observed in the field.

2.3 Dataset generation from simulated echolocation behaviour

To explore how call dynamics scale with approach velocity, we used the `simulateEcholocation` function to generate a synthetic dataset spanning a wide range of velocities. By systematically varying the initial velocity, we obtained a large-scale dataset of simulated call events that preserves the temporal and kinematic dependencies between inter-pulse interval (IPI), distance, and relative speed.

The dataset was generated using a wrapper script (Listing 3), which iterates over a sequence of initial approach velocities from 1 to 20 m/s in increments of 0.05 m/s. The simulator output was parsed for each velocity to extract instantaneous call rate, velocity, distance, IPI, call duration, and amplitude. These parameters were assembled into a long-format table, where each row corresponds to one simulated call event. The resulting dataset was saved as a comma-separated values (CSV) file for further analysis.

```
velocities = 1:0.05:20;   % range of initial velocities
allRows = []; seqNum = 1;

for v0 = velocities
result = simulateEcholocation(bandwidth, kr, target_distance, ...
v0, initial_call_duration, ...
motile, makeAudio);

% Extract outputs
Cr   = min(1 ./ result.delta_t(2:end), result.max_call_rate);
vr   = abs(result.delta_s ./ result.delta_t(2:end));
d    = result.new_target_distance(1:end-1);
ipi  = result.delta_t(2:end);
dur  = result.new_call_duration(1:end-1);
amp  = result.new_amplitude(1:end-1);

% Append to long-format table
row.SeqNum = repmat(seqNum, length(Cr), 1);
row.InitialVelocity = repmat(v0, length(Cr), 1);
row.Rate      = Cr(:);
```

```
        row.Velocity  = vr(:);
        row.Distance  = d(:);
        row.IPI       = ipi(:);
        row.CallDur   = dur(:);
        row.Amplitude = amp(:);
        T = struct2table(row);
        allRows = [allRows; T]; %#ok<AGROW>

        seqNum = seqNum + 1;
        end

        writetable(allRows, 'simulation_results.csv');

```

Listing 3: Dataset generation by iterating the echolocation simulator across velocities. Outputs are collated into a long-format table for each velocity and saved to disk.

The resulting dataset contained over 13,000 simulated call events across the tested velocity range. We processed the aggregated table to analyse emergent patterns and compute correlations between behavioural parameters, including velocity, distance covered, IPI, and call duration. Outliers due to ceiling effects at the maximum call rate or floor effects at the minimum call duration were removed through threshold filtering. Subsampling ensured tractable visualisation while maintaining statistical representativeness. Six representative relationships are illustrated in Figure 9, highlighting how the responsivity framework constrains interdependencies between kinematic and acoustic parameters. The simulated patterns provide a direct benchmark for comparison with analogous relationships derived from field data.

A subset of the dataset was generated under stationary and motile prey conditions using the same simulation procedure to validate the velocity-call rate trade-off relationship. The results of this comparison are shown in Figure 6.

2.4 Spatio–Temporal Parameter Sweep

We performed a two-dimensional parameter sweep to explore how derived biosonar parameters depend jointly on flight velocity and the responsivity coefficient k_r. The simulator function was executed across a grid of initial velocities (3–7 m/s) and k_r values (3–7), with all other parameters constant. From each simulation, the following quantities were extracted: (i) the reaction time threshold, measured at prime responsivity (T_{b^*}), (ii) the total time to contact (until the bat reaches the target), (iii) the value of T_b at the point of prime responsivity R^*, and (iv) the distance to the target at R^*.

These measures were assembled into velocity–k_r matrices and visualised using contour maps (Figure 5b). This approach provides a compact overview of the spatio-temporal constraints deduced by the responsivity framework, showing how call timing and target range estimates vary systematically with the interaction of flight speed and call rate scaling.

2.4.1 Simulation Output

Call–Echo Sequences with Event Markers To illustrate the temporal dynamics of simulated echolocation behaviour, we extracted the echolocation simulator's synthetic call and echo streams. The program returns a two-channel audio vector (`result.audio`), where the first column corresponds to the emitted call sequence and the second to the returning echoes, aligned at the sampling frequency $f_s = 192$ kHz. The onset times of calls and echoes were retrieved from the

vectors `result.call_points` and `result.echo_points`, respectively, providing sample-precise markers of emission and echo arrival.

The audio waveform was normalised and plotted for each velocity condition against time, with vertical markers indicating key events. This representation makes explicit the progressive shortening of echo delays with decreasing target distance and highlights the transition to high-rate buzz calls at short range. Across velocities, these call–echo sequence plots provide a compact overview of how the responsivity framework shapes the temporal structure of biosonar behaviour. The call-echo time-series plots are depicted in Figures 2c & 7. An example spectrogram of the simulated call-echo pairs is presented in figure 3c. Further, the output data is also used to represent the reaction time windows as a function of velocity and responsivity coefficient in Figure 5a.

2.5 Derived Scaling Relationships

2.5.1 Relationship Between Call Rate and Relative Motion

Within the responsivity framework, the timing of calls is regulated by the echo delay T_a. The inter-pulse interval (IPI/Δt) is scaled by the responsivity coefficient k_r, such that

$$\Delta t = T_a(1 + k_r).$$

This formulation captures the degree to which the bat prolongs or compresses the waiting time between successive calls relative to the echo return. The call rate is the reciprocal of the IPI,

$$C_r = \frac{1}{\Delta t} = \frac{1}{(1 + k_r)T_a} = \frac{c}{2d(1 + k_r)} \tag{19}$$

Thus, C_r decreases with increasing distance to the target and increases with decreasing d, while k_r modulates the sensitivity of the loop. When $k_r \to 0$, call rate is tightly coupled to echo delay, while larger k_r values yield slower updates. This expression provides a direct quantitative link between relative motion, target distance, and the responsivity of the call–echo loop.

2.5.2 Call Rate Modelling Across Target Distance

To examine how call rate scales with echo delay and reaction time, we modelled the expected call rate C_r as the inverse of the combined echo delay and biological reaction window. We applied the same definitions of T_a and T_b from Section 2.1.2, and systematically varied their ratio. By exploring a range of k_r from 0.25 to 10, we derived families of call rate curves that describe how temporal constraints compress as the bat approaches a target.

The resulting model predicts a set of call rate–distance relationships, as presented in figure 1b. These curves illustrate how different assumptions about biological reaction time shift the onset and steepness of call rate acceleration. Notably, the formulation highlights that the maximum call rate is not reached directly as a function of distance, but through the relative scaling of echo delay and neural processing time. This provides a generalised framework to compare simulated dynamics with empirical data.

The curves can also be used to estimate the responsivity coefficient k_r by matching predicted values with observed call rates at known target distances, or to approximate $C_{r,\max}$ when

empirical maxima are uncertain.

Rate of Change of Target Distance. Differentiating the expression 19 with respect to time provides an explicit connection between call rate and the contraction of distance:

$$\frac{dC_r}{dt} = -\frac{c}{2(1+k_r)} \cdot \frac{1}{d^2} \cdot \frac{dd}{dt}, \tag{20}$$

where $\frac{dd}{dt} = \dot{d}$ is the relative velocity between bat and prey. The negative sign indicates that as the bat closes in on the target ($\dot{d} < 0$), the call rate increases, whereas if the target moves away ($\dot{d} > 0$), the call rate decreases. Hence, the steepness of the C_r–d curve reflects not only distance but also the instantaneous rate of change of distance, providing a mechanistic link between call timing and the dynamics of pursuit.

From Call rate to Relative Velocity. Using

$$C_r = \frac{c}{2d(1+k_r)} \qquad \Longleftrightarrow \qquad d = \frac{c}{2(1+k_r)\,C_r}, \tag{21}$$

The distance dynamics can be written in terms of the call rate. Differentiating the inverse relation gives

$$\dot{d} \;=\; -\frac{c}{2(1+k_r)}\,\frac{1}{C_r^2}\,\dot{C}_r \quad \Longrightarrow \quad v_r \;\equiv\; -\dot{d} \;=\; \frac{c}{2(1+k_r)}\,\frac{\dot{C}_r}{C_r^2}. \tag{22}$$

Equation 22 is the exact continuous-time link between the closing speed and the evolution of call rate. The same expression follows from a discrete step analysis: with $\Delta t \approx 1/C_r$ and $d = \frac{c}{2(1+k_r)C_r}$,

$$\Delta C_r \approx \frac{\partial C_r}{\partial d}\,\Delta d = \frac{C_r}{d}\,(-v_r\,\Delta t) \;\;\Rightarrow\;\; v_r \approx \frac{c}{2(1+k_r)}\,\frac{1}{C_r^2}\,\frac{\Delta C_r}{\Delta t}, \tag{23}$$

which tends to (22) as $\Delta t \to 0$.

Implications for scaling. Equation (22) shows that the *shape* of the empirical v_r–C_r curve depends on how quickly the call rate is adjusted, i.e. on $\dot{C}_r$ as a function of C_r. If the controller updates the call rate according to a power law $\dot{C}_r \propto C_r^{\gamma}$ over a regime (where noise and ceilings are not dominant), then

$$v_r \;\propto\; C_r^{\gamma-2}.$$

Hence a fitted relation $v_r \propto C_r^{b}$ implies $\gamma = b+2$. For example, the commonly observed $b \approx -\frac{1}{2}$ in our simulations is consistent with $\dot{C}_r \propto C_r^{3/2}$, i.e. call-rate updates that accelerate sublinearly with the current rate. Near the buzz ceiling, $\dot{C}_r \to 0$ and equation 22 predicts the flattening seen empirically.

Practical Use. Given k_r and a measured $C_r(t)$ trace, one can estimate instantaneous closing speed directly from call timing:

$$\boxed{v_r(t) \;=\; \frac{c}{2(1+k_r)}\,\frac{d}{dt}\left(\frac{1}{C_r(t)}\right) \;=\; \frac{c}{2(1+k_r)}\,\frac{\dot{C}_r(t)}{C_r^2(t)}} \tag{24}$$

which provides a non-invasive, timing-only estimator of approach velocity that is consistent with the responsivity framework.

2.5.3 Deriving Target Distance from Call Rate

From the responsivity relation between IPI and echo delay (Equations 1–3), the instantaneous distance to the target can be expressed directly in terms of call rate:

$$d = \frac{c}{2(1 + k_r)\, C_r}. \tag{25}$$

Equivalently, using IPI rather than call rate,

$$d = \frac{c \cdot \mathrm{IPI}}{2(1 + k_r)}. \tag{26}$$

This provides a simple analytical route to infer target distance from recorded call dynamics, an identity confirmed in simulation by the close match between the derived d and the ground-truth trajectory (see Figure 4).

2.6 Validation of Derived Responsivity Identities

To test the internal consistency of the responsivity framework, we validated the key analytical identities that link call rate, target distance, and relative velocity. Simulations were run using the `simulateEcholocation()` function, with parameters fixed at a call bandwidth of 45–90 kHz, an initial target distance of 10 m, relative approach velocity of 5 m/s, and responsivity coefficient $k_r = 5$. Motile noise and audio synthesis were disabled to ensure deterministic outputs.

The inter-pulse intervals Δt were extracted and inverted from the simulator output to compute the instantaneous call rate $C_r = 1/\Delta t$. Target distance values were taken before and after each displacement step, while relative velocity was calculated directly as $v_r = \Delta s/\Delta t$. These empirical trajectories were compared against theoretical predictions derived from the responsivity framework:

- The distance identity, $d = c/\big[2(1{+}k_r)C_r\big]$, was tested against simulated distances measured before each step.
- The velocity identity was derived in discrete product form,

$$v_r \;\approx\; \frac{c}{2(1 + k_r)} \cdot \frac{\Delta C_r/\Delta t}{C_r^2},$$

  and compared with the true stepwise velocity.

Validation plots (Figure 4) confirmed close alignment between the simulated and theoretical quantities. Specifically, (I) relative velocity derived from displacement matched that inferred from the call rate product, (II) simulated distances coincided with those obtained from the distance identity, (III) simulated (d, C_r) pairs collapsed onto the analytical hyperbolic curve, and (IV) velocity–call rate relationships overlapped across simulation and discrete theory.

As a further verification, the mean absolute deviation between theoretical and simulated velocities and the median deviation between simulated and reconstructed distances were com-

puted. These metrics verified that deviations remained negligible, confirming the responsivity framework's robustness under discrete simulation.

2.7 Interception Strategy Based on Relative Velocity

2.7.1 Time to Interception as a Function of Relative Velocity

We modelled the time required for a bat (chaser) to intercept a moving target given an initial separation distance d_0. The chaser velocity v_c was fixed at 5 m/s, while relative target velocities v_r were varied between 0.1 and 20 m/s. For each condition, the effective target speed was defined as $v_t = v_c - v_r$, and the target–chaser separation was iteratively updated as:

$$d_{n+1} = d_n - (v_c - v_t) \cdot \Delta t, \tag{27}$$

where $\Delta t = 0.01$ s is the integration step. The simulation terminated when $d \leq 0$ or a maximum time window ($t_{\max} = 50$ s) was reached.

The time to interception T_{int} was recorded for each relative velocity, and the corresponding distance travelled by the chaser was calculated as:

$$D_c = v_c \cdot T_{\text{int}}. \tag{28}$$

Results are plotted as interception time T_{int} versus relative velocity v_r (Figure 1c), illustrating the scaling of pursuit time with prey escape speed. This model provides a simple kinematic estimate of the spatiotemporal constraints on successful interception given known bat velocities and initial separation.

2.7.2 Velocity–Call Rate Tradeoff

A key component of the theoretical model developed in this study is the hypothesis that prey interception behaviour in echolocating bats is governed by the relative velocity between the bat and its target. This relationship is formalised through the derivations in expressions 22 and 24. The relative velocity determines the time window available to complete the sensory-motor loop necessary for successful capture. Assuming the bat emits a call at an initial distance d_0 from the target, the time to interception is given by:

$$t = \frac{d_0}{v_r} \tag{29}$$

This inverse relationship forms a rectangular hyperbola (Figure 1c & 7), such that small relative velocities lead to extended interception durations. In contrast, higher relative velocities shorten the time available for sonar updates, leading to distinct behavioural outcomes:

$$\begin{cases} v_r = 0 & \Rightarrow \text{chase time } \to \infty \\ v_r \ll v_{\text{bat}} & \Rightarrow \text{long, prominent buzz} \\ v_r \approx v_{\text{bat}} & \Rightarrow \text{short buzz} \\ v_r \gg v_{\text{bat}} & \Rightarrow \text{no buzz} \end{cases} \tag{30}$$

In this context, the buzz, a rapid sequence of short, high-rate calls preceding capture, is a behavioural manifestation of the highest sonar responsivity. When v_r is small, the bat can

accelerate its call rate and achieve prime responsivity well before reaching the target, producing a long buzz. As v_r increases, the bat must reach prime responsivity closer to the target, reducing the length or likelihood of a buzz. In extreme cases where the relative velocity is very high, the adaptation time required to reach the responsivity ceiling may exceed the time to contact, resulting in a complete omission of the buzz. This hypothesis reframes buzz behaviour as an emergent outcome of the dynamic interplay between motion, sensory processing constraints, and environmental predictability. It implies that buzz duration and its occurrence are context-dependent, adapting to the bat's ability to update its spatial model of the target within the confines of echo delay and processing time. This hypothesis is examined through both simulations and field data in subsequent sections.

2.8 Field Data Collection and Analysis

2.8.1 Recording Setup

We collected acoustic data to validate the simulation predictions using a four-channel microphone array in a natural foraging environment (Weihenstephan, Freising, Germany, August - September 2021).

The schematic diagram of the setup is shown in Figure 3a. An assembled array of four microphones was installed in the indicated position, marked in numbers. The three arms of the array were made of straight wooden strips with a 2 cm square profile. A triangular junction crafted out of wood held the arms in position. The arms could be slipped out by loosening the junction fastener, thus making the setup portable. The junction was mounted on a ball joint as a provision for angular positioning of the array, if necessary. All the surfaces on the array were covered in absorptive foam.

The array was mounted on a studio lighting tripod, extendable up to 3 m, providing enough ground clearance and reaching high enough to face the foraging bats.

The microphones (custom-designed with Knowles SPU0410LR5H-QB) were calibrated against a $\frac{1}{4}''$ B&K reference, and the recording program included a frequency domain signal calibration filter to convolve the incoming signal before writing to uncompressed `.wav` files. The system was powered by 12 v car batteries with a DC-AC inverter supplying the computer and the audio interface. Our recording program included a method to trigger the recording based on signal monitoring, and a recording extension was incorporated to extend the recording if there was call activity in the final seconds of the initially set ceiling of 10 s.

High-quality bat activity sequences were selected based on a signal-to-noise ratio (SNR) threshold of 30 dB. Of over 380 sequences, 35% contained at least one buzz. Extracted calls were manually verified and processed to exclude extracted ground reflections and low SNR calls.

2.8.2 Trajectory Reconstruction and Call Parameter Extraction

Localisation and flight trajectory reconstruction were performed using a custom MATLAB class, and call parameters (e.g., rate, duration, amplitude), 3D positions and bat velocity profiles were computed. We used the Time-Difference of Arrival (TDoA) method (cf. [19]) to localise the sound source in 3D. Further quality control was implemented to exclude localisation data points exceeding 8m in any direction, as localisation confidence reduces at increasing distances.

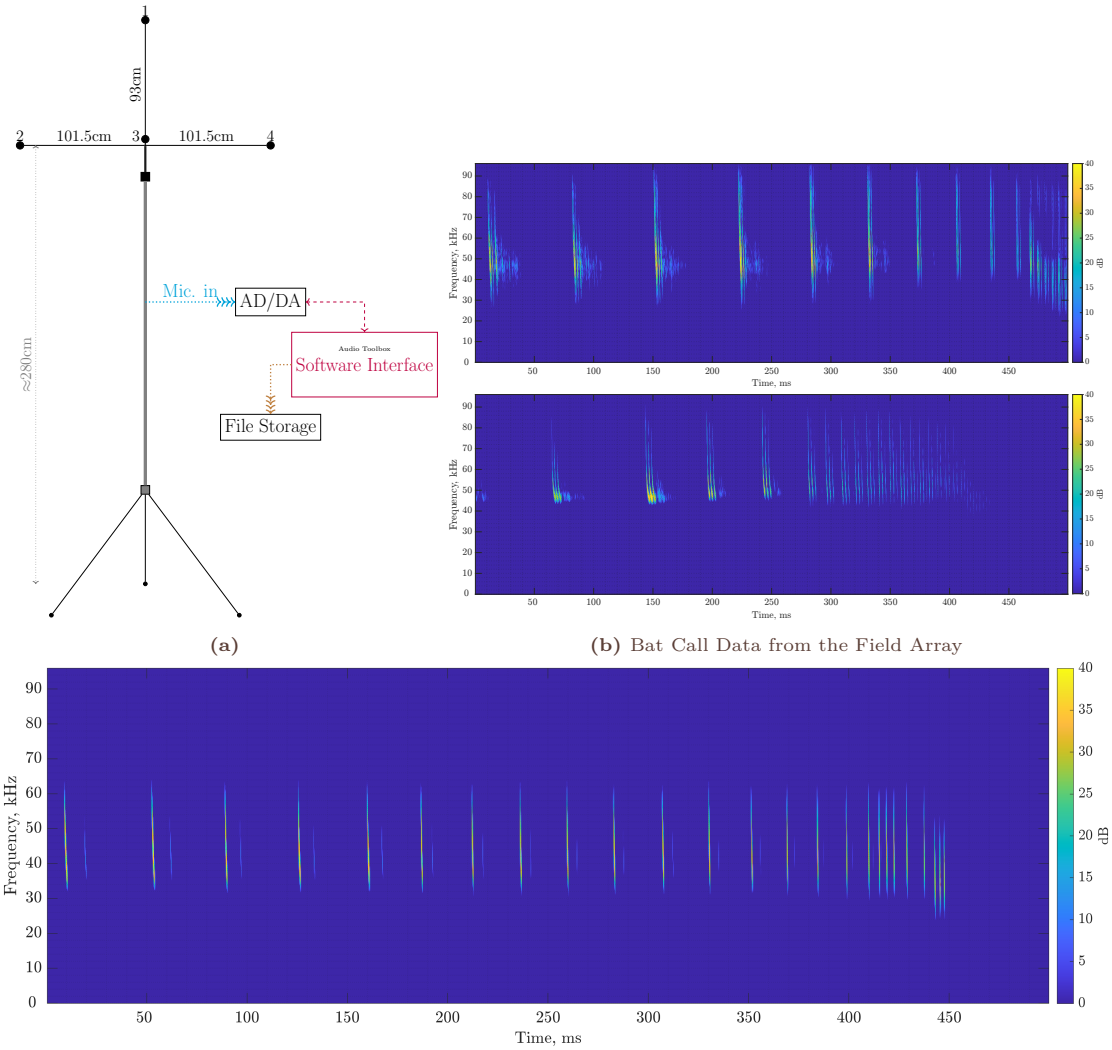

(a)

(b) Bat Call Data from the Field Array

(c) Spectrogram of Simulated Call Sequence

Figure 3: Field and Simulated Primary Data. (a) Field Array Setup. We custom-built a microphone array for easy deployment and high-quality recordings. Four custom-designed Knowles MEMS microphones were calibrated against B&K reference microphones, and the incoming signal was convolved with a calibration filter before writing to the disk. **Comparison between real and simulated echolocation data. (b)** shows echolocation call sequence data from the field array, the two different species (*Myotis sp.* & *Pipistrellus sp.*) of bats foraging at the recording site. **(c)** presents a simulated echolocation call-echo sequence as a spectrogram. Note that the echoes in the field data are ground reflections reaching the microphone, not the target echoes reaching the bat as in the simulated sequence. The placement of echoes in the simulated sequence is governed by the echo delay T_a, and the echo level depends on the source level and the target strength. In the presented spectrogram, the echoes are extremely faint, as expected. The time sequence plots presented in figures 2c & 7 highlight the echoes better.

2.8.3 Statistical Analysis and Model Comparison

Power-law regression was applied to simulation and field data to assess the velocity and call rate relationship. A clustering algorithm (DBSCAN) [21] was used to examine the density and distribution of data points in the velocity-call rate domain–implemented using `dbscan` function in Matlab. Sparse regions in the upper diagonal domain were flagged as areas where high velocity and high call rates rarely co-occurred.

The model's prediction of buzz readiness timing and its dependence on relative velocity were compared against the field-recorded data to validate the alignment between theory and observation.

All data analysis and visualisation were performed using MATLAB R2023b.

3 RESULTS

3.1 Validation of Derived Parameters

The validation analysis confirmed that the responsivity framework yields self-consistent predictions across its derived quantities (Figure 4). Relative velocity computed directly from the simulator as $\Delta s/\Delta t$ closely matched the value reconstructed from the discrete product form of call rate (Figure 4.I), with mean deviations below 0.05 m/s. The distance identity $d = c/\left[2(1+k_r)C_r\right]$ reproduced the simulated target distances with negligible error (median deviation < 0.0001 m), demonstrating that target range can be recovered from call rate alone (Figure 4.II).

Similarly, plotting simulated (d, C_r) pairs showed excellent alignment with the theoretical hyperbolic relationship $C_r(d)$ (Figure 4.III). Finally, the relationship between velocity and call rate revealed consistent overlap between simulator-derived values and the discrete theoretical form (Figure 4.IV), further confirming the internal coherence of the framework.

These results demonstrate that the responsivity framework preserves strict mathematical consistency between distance, velocity, and call rate. The negligible discrepancies observed are attributable to discrete sampling effects in the simulation rather than violations of the underlying theoretical identities.

3.2 Spatio–Temporal Parameter Profiles

The parameter sweep revealed systematic interactions between flight velocity and responsivity coefficient k_r (Figure 5). The characteristic fastest reaction window T_{b^*} remained within a narrow range (4.4–5.5 ms), showing only modest variation across the parameter space. By contrast, the time to contact decreased steeply with both increasing velocity and k_r, reflecting the accelerated approach dynamics and slower processing.

At the point of prime responsivity R^*, T_b exhibited a broad dynamic range, spanning from $\sim$20 ms at low velocities and k_r to less than 10 ms at higher values. The corresponding distance to the target at R^* also decreased systematically, with larger values (> 2 m) occurring at low velocity and low k_r, and distances below 0.5 m when both parameters were elevated.

In addition, the reaction time window available to the bat at each call was derived as $T_b = k_r \times T_a$, (Figure 5a). Across initial velocities of 3–5 m/s and a range of k_r values, T_b decreased sharply with successive calls, converging towards a narrow window near the buzz phase. Markers for the maximum call rate (black dots) and the onset of call–echo overlap (red dots) indicate

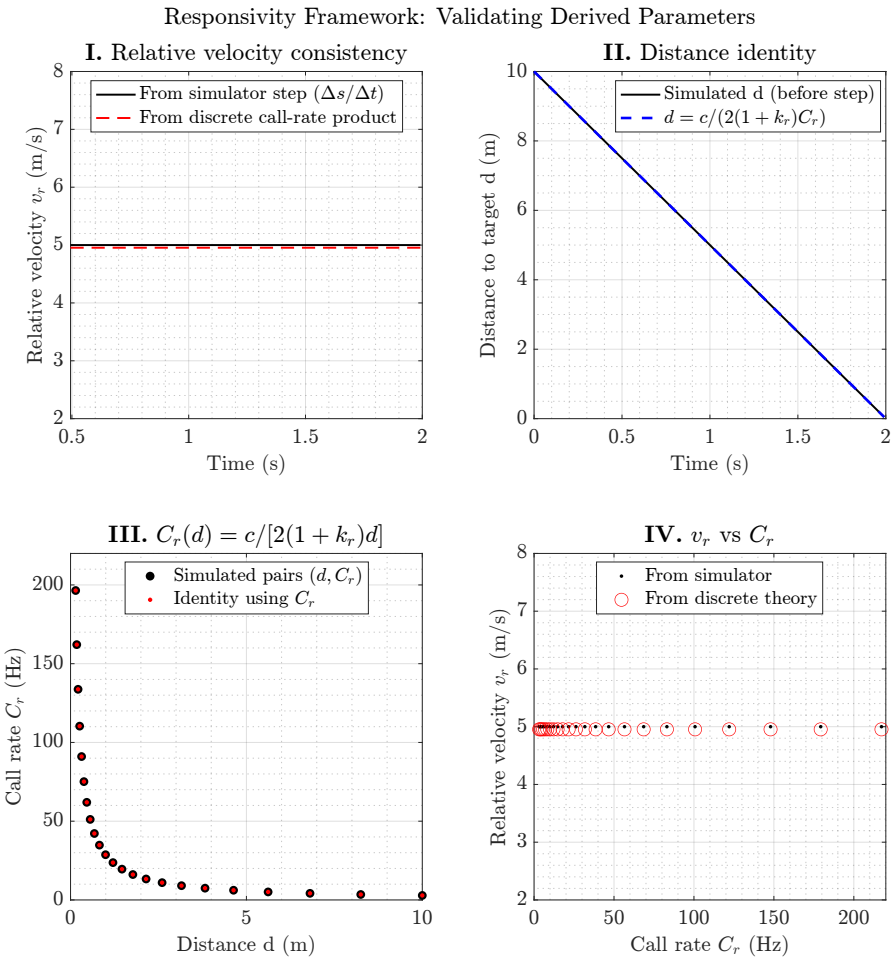

Figure 4: Validation of responsivity framework equations. Relationships among derived parameters were cross-checked against simulation outputs. (**I**) **Relative velocity consistency:** The velocity estimated directly from displacement per step ($\Delta s/\Delta t$, black) closely matches the theoretical value reconstructed from the discrete product form of call rate (red dashed). (**II**) **Distance identity:** Simulated pre-step distances d (black) are indistinguishable from those recovered using the identity $d = c/[2(1+k_r)C_r]$ (blue dashed). (**III**) **Call rate vs. distance:** Simulated (d, C_r) pairs (black points) align with the theoretical hyperbolic form $C_r(d) = c/[2(1+k_r)d]$ (red). (**IV**) **Velocity vs. call rate:** The inverse scaling of velocity and call rate derived from the simulator (black) is consistent with discrete theoretical predictions (red). Quantitatively, the mean deviation between simulated and theoretical velocities was < 0.05 m/s, and the median distance error was < 0.0001 m, indicating that the framework preserves strict internal consistency across distance, velocity, and call rate identities.

that these critical transitions consistently occur at short T_b, leaving only a limited time margin for sensory processing and motor responses. This analysis complements the parameter sweep, reinforcing that the interaction of velocity and responsivity dictates the timing of individual calls and bounds the overall decision-making window available to the bat during target interception.

Together, these results demonstrate how the responsivity framework imposes strong joint constraints on temporal and spatial parameters, such that the scaling of call rate with echo delay governs instantaneous timing and determines the range at which critical behavioural transitions occur.

3.3 Velocity–Call Rate Tradeoff: Simulation vs Field Data

Both clean and noisy simulations produced a strong inverse relationship between call rate and relative velocity, described by a power-law of the form $v_r = KC_r^b$. For the clean simulation, the scaling exponent was $b = -0.43$ with prefactor $K = 9.53$ (95% CI: $b \in [-0.46, -0.39], K \in$

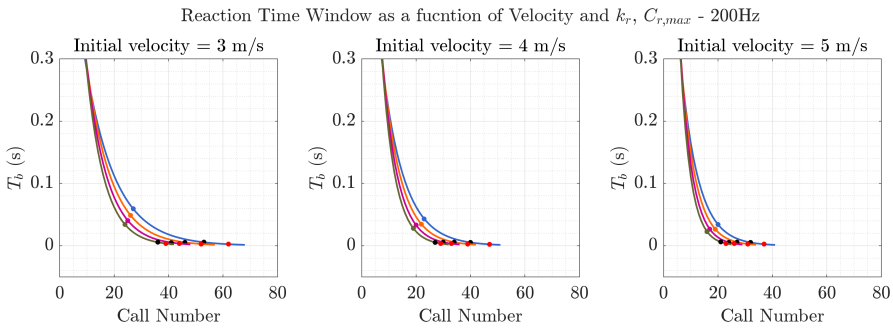

(a)

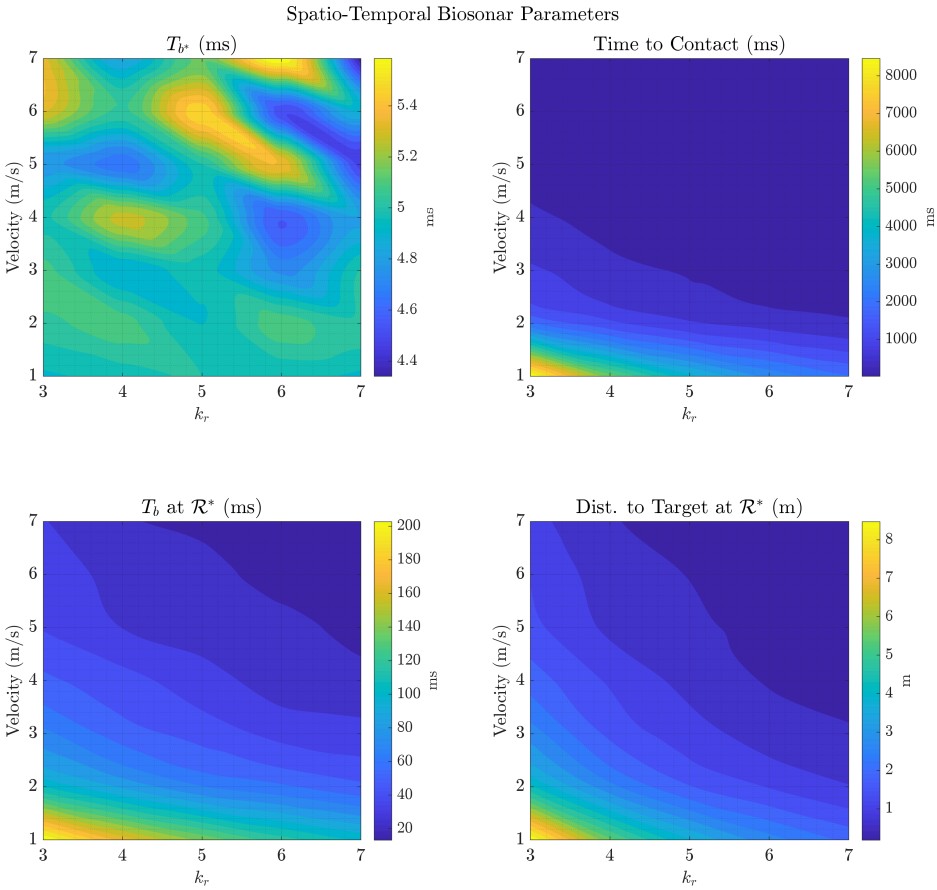

(b)

Figure 5: (a) Biological Reaction Time Window. The reaction time window available at every call may be calculated by knowing the biological reaction constant k_r (refer to Figure 1b) as $T_b = k_r \times T_a$. The echo delay T_a depends on the bat's velocity relative to the target. Here, T_b is calculated for a range of k_r and relative velocities and the available reaction time at the time of reaching the buzz readiness is marked with a dot of the same colour as the line. The line colours correspond to k_r =4-blue, 5-orange, 6-magenta, 7-olive. The point of maximum call rate is marked by a black dot, and the point of call-echo overlap by a red dot. **(b) Spatio-Temporal Biosonar Parameters at Velocity and k_r Combinations.** The four plots here present the following parameters for combinations of relative velocity and k_r, from top left, clockwise, reaction time threshold T_{b*}, time to contact, distance to target at the time of buzz readiness and the available reaction time window. The plots highlight that with increasing velocity and slower response (higher k_r), the spatio-temporal parameters shrink, thus affecting the rate of sensory information update and the favourable conditions for a successful interception.

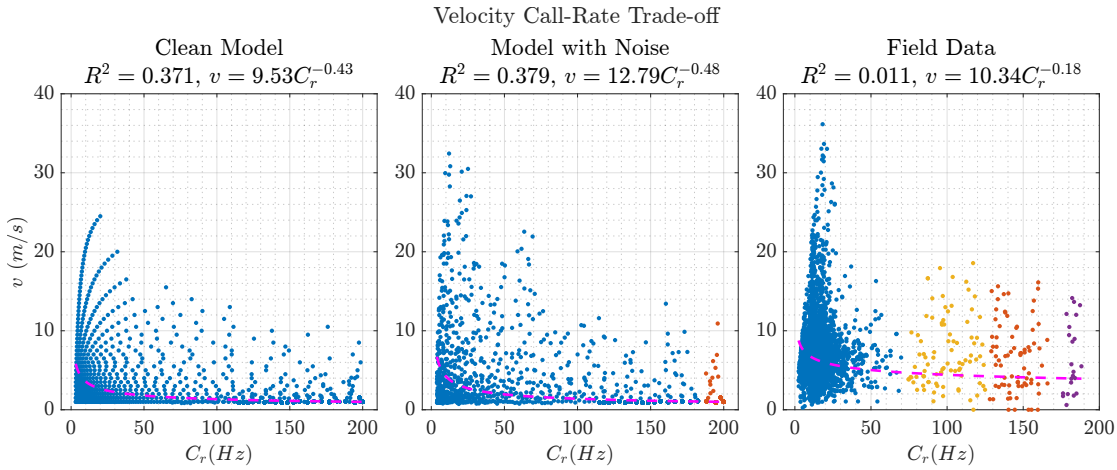

Figure 6: Velocity–call rate trade-off in simulated and empirical data. Power-law fits ($v = K \cdot C_r^b$) are shown for the clean simulation (left), noisy simulation (middle), and field data (right). Both simulation runs converged on consistent negative scaling exponents ($b \approx -0.45$), confirming that relative velocity decreases as the call rate increases according to the responsivity framework. Although the field data yielded a shallower slope ($b = -0.18$) and lower fit quality ($R^2 = 0.01$), the overall trend remains in agreement: bats reduce relative velocity as call rate increases. Bootstrap-derived 95% confidence intervals supported the robustness of the simulated scaling while highlighting broader variability in the field data. Coloured clusters represent DBSCAN-identified point groupings, with four primary clusters in the field dataset.

[8.14, 11.28]), yielding $R^2 = 0.37$. The noisy simulation showed a slightly steeper slope ($b = -0.48$, $K = 12.79$, 95% CI: $b \in [-0.52, -0.45], K \in [10.78, 15.16]$; $R^2 = 0.38$), indicating that proportional Gaussian perturbations do not disrupt the underlying velocity–call rate relationship.

In contrast, the field data exhibited a much shallower slope ($b = -0.18$, $K = 10.34$), with wide confidence intervals ($b \in [-0.36, -0.04], K \in [7.18, 16.16]$) and a poor fit ($R^2 = 0.01$). This suggests that although bats in the field broadly follow the predicted inverse scaling, environmental and behavioural variability reduce the strength and precision of the relationship compared with the controlled simulation. A likely source of this variability is the limited accuracy of acoustic localisation with the planar array, which introduces error into instantaneous velocity estimates [19].

Another factor influencing the discrepancy is the distribution of data points in the field recordings. Whereas the simulations provide balanced sampling across the full range of call rates, the field dataset is heavily biased towards low call rate values, with relatively sparse and dispersed points in the high call rate regime. This imbalance reduces the leverage of the high-rate region, increasing uncertainty in the power-law exponent and contributing to the weak overall fit. Nonetheless, the overall distribution still exhibits a qualitatively consistent inverse trend, which agrees with the responsivity framework's predictions.

Finally, the bootstrap analysis confirms that the simulated scaling laws are robust to stochastic perturbations, whereas field conditions impose greater variability in slope and prefactor estimates.

3.4 Velocity–Call Rate Tradeoff: Event Occurrence Times

Figure 7 visualises the timing of key sonar events during approach: the point of target detection (black line), the onset of call duration contraction (orange line), the peak call rate or buzz readiness (blue line), and the point where call-echo overlap occurs (red line). At slower velocities (1-3 m/s) (panels a, b, c), these events are well-separated, providing a large buffer for sonar

adaptation - the responsivity peak and buzz readiness are reached with ample margin, resulting in long buzz sequences. As velocity increases, the time between these events compresses, and in extreme cases, the responsivity threshold is reached after the echo overlap, eliminating the possibility of an effective buzz. In contrast, the sonar update window is compressed with increasing velocities (panels d, e, f, g). At higher velocities such as 10-15 m/s, as shown in Figures 7f-7h, the responsivity threshold was reached only near or after the point of contact with the target, effectively precluding the production of a structured buzz. The time-to-intercept curve (Figure 1c) explains this trend, showing a hyperbolic decay in available time as velocity increases.

3.5 Comparison of Field and Simulated Behavioural Profiles

To evaluate whether the responsivity framework can reproduce the behavioural structure observed in echolocating bats, we compared parameter profiles derived from field recordings with those generated through simulation (Figures 8, 9). Both datasets reveal consistent interdependencies between call rate, call duration, and inter-pulse interval (IPI). Specifically, the expected inverse scaling between call rate and call duration is robustly recovered in both empirical and simulated data (panels c–d), and within-sequence variation in call duration shows the predicted trade-off with IPI (panel f).

The main divergence arises in the relationship between call duration changes and inter-call distance (panel e). In the simulation, the true relative velocity of the bat with respect to the target is explicitly known, yielding a systematic correlation between call duration and distance covered. By contrast, inter-call displacement must be reconstructed from acoustic localisation relative to the array in the field data. This procedure provides only the estimated ground speed. It is sensitive to tracking errors, especially at longer distances and lower signal-to-noise ratios and the geometry of the microphone array as established in our previous study [19]. Consequently, noise in positional estimates obscures the underlying relationship, producing weaker and more variable associations in the field profile.

Taken together, the results demonstrate that the responsivity model reproduces the key acoustic trade-offs observed in natural recordings, while also highlighting how measurement limitations in field conditions — particularly localisation accuracy — contribute to the additional scatter and reduced explanatory power in the empirical dataset.

4 DISCUSSION

The present study develops and validates the *responsivity framework*. This mechanistic model links call rate dynamics in echolocating bats to relative velocity, echo delay, and spatial constraints of target approach. The framework captures how bats regulate sonar timing under biophysical and neural constraints by formalising the proportional scaling between echo delay and inter-pulse interval through the responsivity constant k_r. Using simulations, we demonstrated the model's internal consistency, recovering fundamental identities relating distance, velocity, and call rate, and generating synthetic behavioural profiles that closely parallel field recordings. Comparisons with empirical data revealed strong qualitative agreement and predictable deviations from localisation noise and sampling biases, highlighting the framework's utility in separating intrinsic control structure from measurement artefacts.

Beyond these specific results, the framework articulates a general principle: the tempo of

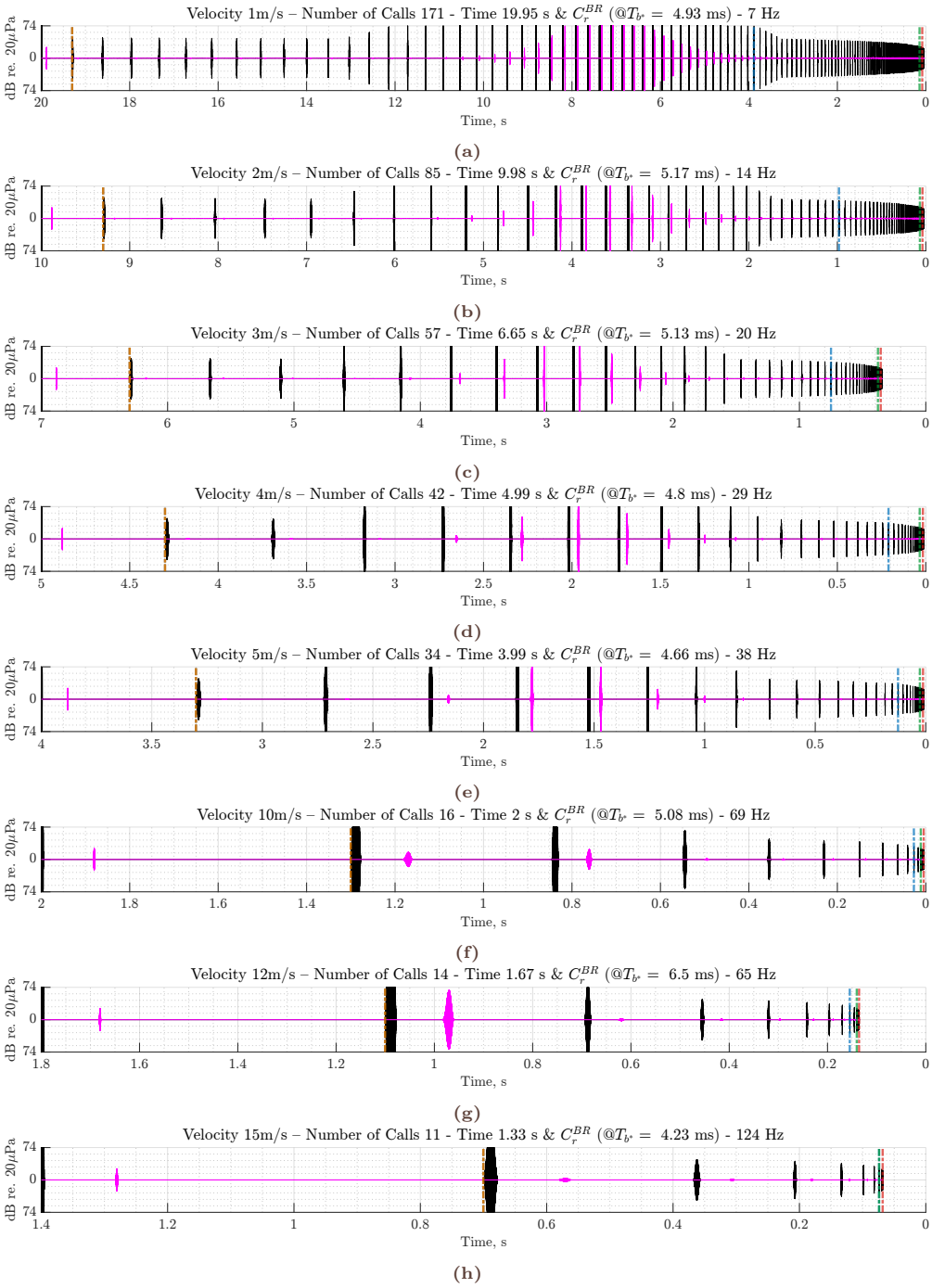

Figure 7: Velocity–Call Rate Tradeoff. Each panel corresponds to an initial velocity value in a simulated echolocation call sequence with a stationary prey target ($d = 20$ m). The panel titles indicate the number of calls required to reach the target, the total sequence duration, the total time of the sequence, and the call rate at buzz readiness with the fastest available reaction time. At higher approach velocities, fewer calls are produced, and the buzz readiness threshold ($\mathcal{R}^*$, blue line) is reached much closer to the target. This reflects a key constraint: the bat cannot sufficiently increase call rate earlier in the sequence without reducing flight speed. Call–echo pairs are plotted in black and magenta, respectively. Event markers: black – target detection (echo level >20 dB), orange – onset of call duration contraction, blue – buzz readiness ($\mathcal{R}^*$), green – maximum call rate ceiling (200 Hz), and red – onset of call–echo overlap ($T_b = 0$). The simulations assume a constant velocity for analytical simplicity, and the prey is stationary. Thus, the inverse relationship between call rate and velocity arises directly from echo delay dynamics underpinned by the responsivity coefficient k_r. As velocity increases, the buzz as a distinct feature disappears into the final calls, illustrating the physiological and biomechanical trade-off between approach speed and temporal sampling rate.

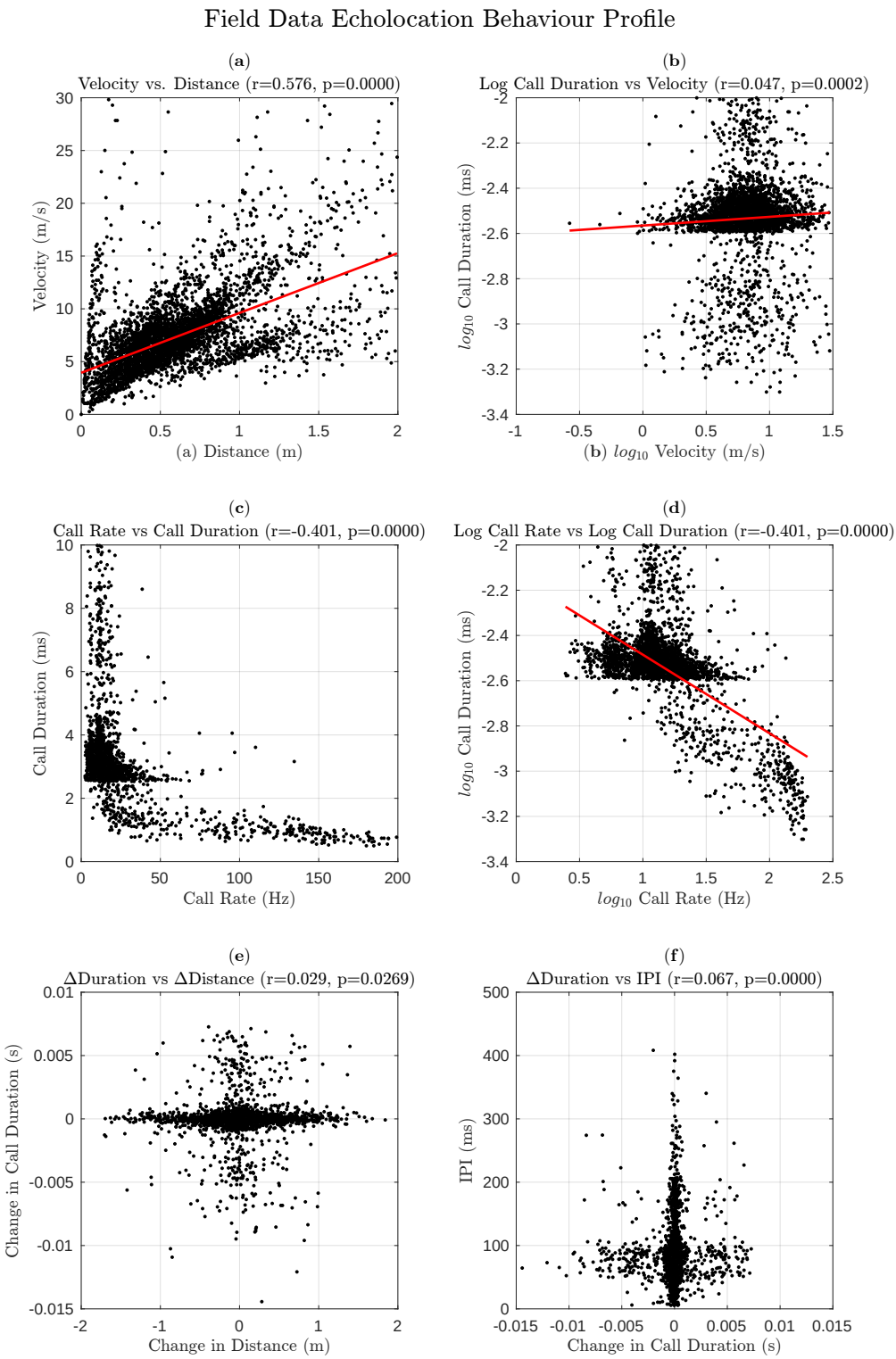

Figure 8: Field Data Echolocation Behaviour Profile. Relationships between flight kinematics and acoustic parameters measured from foraging bats. (**a**) **Velocity vs. Distance**: The distance travelled between calls increases systematically with flight speed. (**b**) **Log Call Duration vs. Velocity**: A very weak but significant positive correlation suggests that higher velocities are associated with marginally longer call durations. (**c**) **Call Rate vs. Call Duration**: Call durations are constrained at high call rates, reflecting the physiological limit of pulse–echo processing. (**d**) **Log Call Rate vs. Log Call Duration**: The same inverse relationship expressed in log–log space, highlighting a clear power-law trend. (**e**) **ΔCall Duration vs. ΔDistance**: No consistent correlation between within-sequence changes in call duration and inter-call distance, suggesting largely decoupled control of these parameters. (**f**) **ΔCall Duration vs. IPI**: Changes in call duration show little systematic relation with the inter-pulse interval (IPI), indicating independent adaptation of these two temporal parameters.

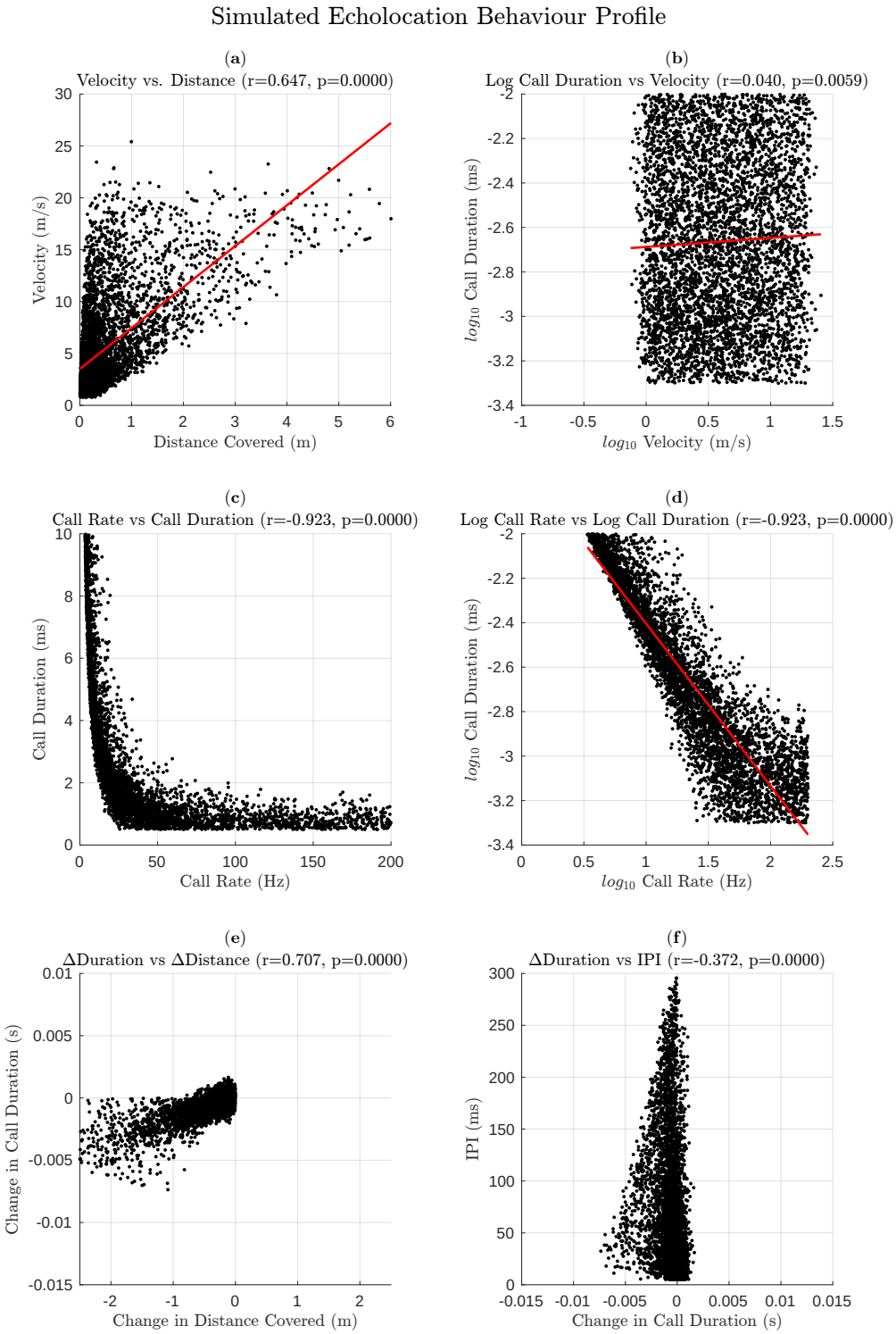

Figure 9: Simulated Echolocation Behaviour Profile. Behavioural relationships generated from the responsivity framework simulation are plotted in the same format as the field data for direct comparison. (**a**) **Velocity vs. Distance:** In the simulation, the target distance is explicitly known, and velocity is computed as the instantaneous relative approach speed. This contrasts with field data, where velocity is estimated as ground speed from localisation, leading to differences in the scaling of distance travelled per call. (**b**) **Log Call Duration vs. Velocity:** A marginal but consistent positive correlation is recovered, in agreement with the field profile. (**c**) **Call Rate vs. Call Duration:** The expected negative correlation is strongly expressed, reflecting the physiological coupling of call rate and duration. (**d**) **Log Call Rate vs. Log Call Duration:** The same relation plotted in log–log space reveals a clear power-law dependence. (**e**) **ΔCall Duration vs. ΔDistance:** In contrast to the field data, the simulated relative velocity yields a systematic positive correlation, with longer calls associated with larger distances travelled per step, and shorter calls linked to smaller displacements. (**f**) **ΔCall Duration vs. IPI:** A negative association is observed, such that increases in call duration coincide with shorter silent intervals (IPI), while decreases in call duration extend the IPI – consistent with the prediction that call timing and duration jointly partition the available reaction window. Overall, the simulated dataset reproduces the same behavioural profiles observed in the field except panel (e), where the exact knowledge of relative velocity leads to a stronger systematic trend compared to localisation-derived field measurements.

adaptive behavioural adjustments is limited by the speed of the regulatory feedback that governs them. In echolocation, call rate adaptation is bounded both by the neural–motor loop's latency and by the finite speed of sound propagation, such that interception strategies emerge from the interplay between physical motion and physiological reaction time.

Together, these results position the responsivity framework as a unifying principle for understanding the temporal organisation of echolocation behaviour, providing explanatory power for classic phenomena such as the buzz, while offering predictive tools to interpret cross-species differences and to design targeted experimental manipulations.

4.1 Derivations, Parameters and Validations

4.1.1 Responsivity coefficient k_r

The responsivity coefficient k_r defines the proportionality between the acoustic travel time T_a and the inter-pulse interval T_b, expressed as $T_b = (1 + k_r)T_a$ (Figure 1a). This parameter is central to the framework, as it constrains how rapidly the call rate adapts with decreasing target distance (Figure 1b).

Theoretical predictions show that k_r directly determines the curvature of the call rate vs. distance function (equation 19 & Figure 4.III). Simulation outputs confirmed that the simulated (d, C_r) pairs matched the theoretical hyperbolic form with negligible error (median deviation < 0.0001 m; Figure 4.III). Thus, k_r can be interpreted as a physiological tuning parameter: higher values imply sluggish adaptation of call rate to decreasing distance. In contrast, low values enforce steeper temporal adjustments, potentially reflecting differences in neural integration time or sensory–motor coupling.

4.2 Neural correlates of the responsivity coefficient k_r

Although the circuit basis of *responsivity* requires targeted physiology, converging evidence from cortical neurophysiology suggests that k_r can be interpreted as a population-level gain on the echo-delay–to–call-timing transform.

Classical work by Suga and Horikawa (1986) [22] demonstrated that delay-tuned neurons in the moustached bat cortex exhibit systematic echo-delay tuning but non-uniform response latencies. In the FM–FM area, first-spike latencies clustered tightly around ∼9 ms, whereas neurons in the dorsal fringe (DF) region displayed a broader, bimodal distribution with peaks near ∼9 ms and ∼24 ms, extending in some units to ∼40 ms. This distribution implies that echo-delay representation arises from a population code with variable integration times rather than a uniform latency anchor, consistent with the interpretation that the responsivity coefficient k_r reflects circuit-level modulation of temporal gain across neurons with different echo-delay preferences.

Pulse rate-dependent retuning of delay sensitivity. Studies by Wong et. al (1992) [23] show that in the auditory cortex of the FM bat *Myotis lucifugus*, most neurons exhibit delay sensitivity, but their tuning sharpens and can degrade at high pulse-repetition rates (PRRs, or call rate). Importantly, a distinct class of *tracking neurons* systematically shifts its best delay as PRR increases, effectively following the operating point of the sonar loop [23] (also see Suga et. al. (1983) [24]). This PRR-contingent retuning provides a concrete neural analogue of k_r: as

the bat tightens its emission schedule (shorter IPIs), parts of the cortical population compress their effective temporal integration so that echo-anchored timing remains informative at higher update rates. In our terms, increasing PRR corresponds to reducing the echo delay T_a, and the observed tracking of best delay is consistent with a larger responsivity gain that shortens the reaction window T_b in proportion to T_a (cf. equation. 2). *Tracking* thus maps naturally onto responsivity-driven control, rather than a fixed-delay code. (See also the narrowing/loss of delay tuning at high PRR and the prevalence of tracking units reported in Wong et. al (1992) [23].)

Population remapping with echo-acoustic flow. At the mesoscale, approach dynamics (echo-acoustic flow) reshape the cortical representation of target range, enhancing short-delay coding as range closes, and more prominently at higher approach speeds, as shown by Bartenstein et al. (2014) [25]. This dynamic reweighting of the range map provides a population mechanism to realise a context-dependent reaction time – when approach accelerates, the network increases gain on short delays, compressing the effective processing window and promoting high-rate control [25].

Echo-anchored timing during approach. Classical work on neural image formation during target approach by Dear et. al. (1993) [26] shows that delay-tuned population activity evolves with the closing range, consistent with spike timing that is more stable with respect to *echo* arrival than to *call* onset. In our framework, this is exactly what one expects if $T_b = (1+k_r)T_a$ – absolute response latencies (call-locked) shift with T_a, while echo-locked timing remains narrow. The decision signal (e.g., a pooled-rate bound crossing) would then occur $\approx k_r T_a$ after echo arrival, yielding the observed contraction of the control window near buzz readiness [26].

Taken together, latency distributions in delay-tuned neurons, PRR-contingent retuning at the single-unit level, population remapping with echo-acoustic flow, and echo-anchored timing during approach are all signatures of a circuit that *scales its integration time with echo delay.* This is precisely the neural computation k_r captures in the responsivity framework: a context-dependent gain that converts sensory delay into a motor-updated emission schedule.

4.2.1 Reaction window T_b

The processing interval T_b defines the biological reaction window available to the bat for processing echoes and updating motor responses (Figure 5a). As velocity and k_r increase, T_b contracts rapidly, thereby reducing the time available for sensory–motor integration at the buzz readiness point, or prime responsivity $\mathcal{R}^*$. The role of velocity scaling is also evident from the interception curves (Figure 1c), which show how higher approach speeds dramatically reduce the remaining time-to-contact, thereby tightening the effective T_b window.

The spatio-temporal maps (Figure 5b) highlight this constraint: T_{b^*}, the shortest available reaction window, remains narrowly confined (4.4–5.5 ms) across parameter space. At the same time, the time-to-contact at $\mathcal{R}^*$ shrinks sharply with increasing velocity and higher k_r. At the point of prime responsivity $\mathcal{R}^*$, T_b exhibits a broad dynamic range: $\sim$200 ms at low velocity/k_r values, but collapsing below 20 ms under higher value pairs. This indicates that T_b acts as the ultimate bottleneck of sonar-guided pursuit, and places strong constraints on when a transition into a reactive control regime becomes necessary.

While represented here by a single parameter, the biological reaction window can be decomposed into several discrete stages of neural processing and motor relay, potentially accompanied by an additional voluntary lag (Figure 1a). For analytical tractability, the present models assume a zero voluntary lag, such that T_b represents the minimal effective window. Whether naturally behaving bats insert such voluntary delays into the control loop remains unknown. Moreover, the division of T_b into sensory processing, central integration, and motor execution subcomponents is not known, and their relative proportions may vary across behavioural contexts. Nevertheless, under strictly closed-loop conditions, such as during a reactive control phase, any voluntary lag would be forced away, as temporal efficiency becomes the overriding priority. This formulation therefore provides a conservative estimate of the bat's reaction capacity, anchored in the biophysical limits of the sensorimotor loop.

4.2.2 Buzz readiness

Buzz readiness, defined as the state when call rate adaptation approaches the physiological maximum ($\mathcal{R}_n \approx C_{r,max}$), emerges naturally from the responsivity scaling (Figure 2). The framework identifies this threshold at the point where responsivity $\mathcal{R}$ reaches its minimum (Figure 2a,b), relative to $C_{r,max}$, corresponding to a sharply rising temporal sensitivity.

Anchoring T_{b^*} at $\mathcal{R}^*$ relative to $C_{r,max}$ provides a principled way to project the fastest possible sensorimotor response of the bat onto the rate at which adaptations are converging toward that bound.

This constitutes a form of sensorimotor pre-adaptation: the system does not merely react when the buzz begins, but progressively aligns control dynamics towards the biophysical limit where information updating must saturate. Unlike traditional definitions of the buzz phase, which rely on arbitrary call-rate thresholds (e.g. 150 Hz or 170 Hz), this approach derives directly from the predator–prey dynamic and the finite speed of sound. It is therefore objective, reproducible, and mechanistically grounded in the structure of the sonar feedback loop.

This definition also maps naturally onto established concepts in control theory. In optimal feedback control [17, 27–29], k_r acts analogously to a control gain, dictating how tightly sensory feedback (echo delay) is coupled to motor output (call rate) [17, 28]. In the minimal intervention principle, corrections are made only when they affect task-relevant variables [17, 18]; here, the inflexion point indicates when further shortening of the IPI no longer yields additional benefit, and the system begins to make minimal corrections. In sliding-mode control [30–33], buzz readiness represents a switching surface, where the control policy transitions to a high-gain, saturated regime to maintain stability. From a time-delay systems perspective, the definition identifies the point at which the effective feedback delay (Δt) reaches its minimum controllable bound, directly equivalent to a stability limit. Finally, by formalising $\mathcal{R} = 1/|\Delta\Delta t|$, the framework quantifies the noise–precision trade-off familiar from signal-dependent noise models in motor neuroscience [34].

A further strength of this formulation is that it accommodates multiple inflexion points within a single sequence. In both field and laboratory recordings, bats often produce transient bursts of high-rate calls (sonar sound groups) that do not culminate in a terminal buzz [35]. Traditionally, these have been difficult to interpret, as they temporarily cross high call-rate thresholds without a clear transition criterion. Within the responsivity framework, such transient peaks in responsivity represent moments when prey motion, environmental clutter, or sensory uncertainty

momentarily drive the sonar system toward its control limit. This interpretation aligns with field and laboratory observations by Hulgard and Ratcliffe (2016) [36], who showed that bats produce longer terminal buzzes and more sonar sound groups under higher task complexity–conditions that similarly demand increased sensorimotor precision and control. Thus, the same principle that defines buzz readiness also explains the emergence of sonar sound groups as natural consequences of transient excursions into high-gain regimes.

Thus, defining buzz readiness by anchoring $\mathcal{R}_n$ to $C_{r,max}$ transforms what has previously been an arbitrary phase classification into an objective, mechanistic threshold. It captures both the deterministic constraints of the sensorimotor loop and the adaptive flexibility of bats in natural foraging conditions.

The decrement of call duration with decreasing distance (Figure 1d) provides a mechanistic basis for this transition: shorter calls systematically align with reduced inter-pulse intervals, ensuring that buzz readiness coincides with the steepest segment of temporal adaptation. The simulated call–echo sequences (Figure 2c) show how call duration decrement (orange), buzz readiness (blue), buzz point (green), and overlap onset (red) occur in sequence, thereby marking distinct stages of the terminal approach.

These derivations and validations (Figures 1–5) show that the responsivity framework preserves strict internal consistency while producing biologically interpretable parameters. k_r governs the slope of temporal adaptation, T_b sets the ultimate processing window, and buzz readiness defines the moment sensory–motor control is at an inflexion.

4.3 Distinctions between Simulation and Field Data

Although the responsivity framework is internally consistent and validated by simulation outputs, several vital distinctions arise when comparing with empirical data. These differences primarily reflect methodological limitations of localisation in the field, the nature of the velocity estimates, and the ecological context of foraging behaviour.

4.3.1 Localisation accuracy

In the simulation, target distance and relative velocity are known exactly at each step, so call–echo dynamics can be updated without measurement uncertainty. By contrast, field data rely on acoustic localisation of the bat relative to the microphone array, which introduces errors in reconstructing instantaneous flight trajectories.

4.3.2 Velocity profile

The simulator tracks the *relative velocity to the target*, which is the relevant variable for predicting echo delays and responsivity. Field data, however, yield *ground-referenced velocity*, calculated from changes in the bat's spatial position between calls. Consequently, while the simulation produces smooth monotonic velocity profiles consistent with controlled target approaches, the empirical data often show irregular patterns reflecting opportunistic foraging flights and the absence of a defined prey trajectory. This distinction explains, for example, why the ΔDuration–ΔDistance profiles diverge between simulation and field recordings (compare Figure 9e and Figure 10e).

4.3.3 Idealised pursuit vs. ecological foraging

The simulations present full pursuit sequences, from initial detection to terminal buzz. By contrast, the field dataset is biased toward partial sequences dominated by search, approach, and clutter-related adjustments, with relatively fewer complete terminal pursuits. Further, prey location and movement are unknown, meaning bats adaptively allocate attention to acoustic cues from prey and the distributed clutter in the foraging environment. As a result, call-rate scaling in the field exhibits greater variability, and fits are skewed toward the low call-rate regime where most foraging activity occurs.

Despite this, the overall behavioural profiles remain qualitatively consistent with the responsivity predictions, supporting the generality of the framework while highlighting the ecological factors that reduce quantitative agreement.

4.4 Velocity–Call Rate Tradeoff

The responsivity framework predicts a fundamental trade-off between relative velocity and call rate, which is borne out in both the simulated and field datasets (Figures 6 & 7). In simulation, the predicted inverse scaling relationship emerges robustly, with increasing call rates corresponding to a systematic reduction in relative velocity. This pattern reflects the biophysical constraint that shortening interpulse intervals imposes on the available reaction window, effectively forcing the bat to regulate its speed relative to the target to sustain effective tracking. The framework generates the mathematical form of the velocity–call rate scaling and the predicted boundaries where specific behavioural outcomes, such as the omission of a buzz, become likely.

Figure 7 illustrates how these dynamics play out in complete approach sequences: at lower approach velocities, the temporal spacing between key events—target detection, onset of call duration contraction, buzz readiness, and the ceiling of maximum call rate—remains broad, allowing the bat to sustain long buzz sequences. As velocity increases, however, these events compress into a narrower window, and in extreme cases, the buzz readiness threshold is reached only after contact, effectively precluding the production of a structured buzz. This outcome underscores the necessity of behavioural regulation. Without actively slowing down relative to the target, the bat cannot achieve the optimal interception strategy of reaching maximal responsivity with sufficient time to benefit from high-rate updates. In practice, this means that bats must continuously modulate their flight speed by reducing their forward velocity or adjusting their interception path to ensure that the sonar loop remains within a controllable temporal regime.

The framework thus provides a principled explanation for the varying lengths of buzzes observed in field data. Long buzzes correspond to conditions with low relative velocity, giving ample time for call rate escalation before interception. Short or absent buzzes occur at higher velocities, where the available time collapses, and responsivity thresholds only reach near or beyond the point of capture. These predictions offer a direct mechanistic interpretation of empirical variability: the observed diversity in buzz length is the emergent outcome of a velocity–call rate trade-off governed by the temporal structure of the sonar feedback loop.

4.5 Behavioural Profiles

Behavioural profiles derived from the responsivity simulation and from field recordings (Figures 8 & 9) provide a direct comparison of predicted and observed patterns in the relationships among key echolocation parameters. Each subplot illustrates a distinct aspect of the temporal–kinematic coupling that emerges during target approach.

(a) Velocity vs. Distance Covered. In the simulated data, relative velocity scales positively with the distance traversed between successive calls, as expected from the kinematic constraint that step size is defined by velocity multiplied by interpulse interval. This produces a systematic correlation, with faster approaches yielding larger per-call displacements. In contrast, the distance covered in the field data reflects ground-referenced localisation estimates, which introduce substantial noise and attenuate the expected relationship. The discrepancy reflects the difference between simulated relative velocity (measured directly against the target) and reconstructed ground speed (estimated from bat position relative to the array).

(b) Log Call Duration vs. Velocity. Both simulation and field data reveal a weak positive association, whereby faster flight corresponds to slightly longer call durations. In the framework, this trend arises from the interplay of velocity with call duration decrement rules: at higher speeds, the shortening of interpulse intervals outpaces call duration contraction, producing proportionally longer signals. Although modest in strength, the consistency across datasets suggests this reflects a genuine behavioural adjustment.

(c) Call Rate vs. Call Duration. The well-established inverse relationship between call rate and call duration is strongly expressed in both datasets. In simulation, the curve follows the expected scaling form imposed by the framework, with short durations at high call rates. Field data matches this trend closely, indicating that despite environmental variability, bats adhere to the same fundamental constraint: rapid updates necessitate short signals.

(d) Log Call Rate vs. Log Call Duration. Plotting the same relationship on a log–log scale yields a linearised form highlighting the power-law structure. The simulations reproduce the expected slope, which is consistent with the theoretical scaling. Field data shows greater scatter but conforms to the predicted negative correlation, reinforcing the view that call rate and call duration co-vary under a common constraint.

(e) ΔCall Duration vs. ΔDistance. This subplot reveals one of the most striking differences between the two datasets. In the simulation, relative velocity produces a systematic coupling: smaller per-step distances correspond to shorter call duration changes, expected at higher call rates, yielding a clear positive association. In the field data, however, where displacement is ground-referenced, this relationship is absent, with no consistent trend between within-sequence changes in call duration and estimated distance covered. This discrepancy is attributable to localisation uncertainty and the fact that the prey's location is not directly tracked, making ground-referenced displacement a noisy proxy for relative distance.

(f) ΔCall Duration vs. IPI. In the simulations, a weak negative correlation is present: decreases in call duration are loosely associated with increases in interpulse interval, consistent with the responsivity framework prediction that temporal parameters scale inversely to preserve reaction time. However, the scatter indicates that this relationship is not tightly constrained, even under controlled conditions. In the field data, no systematic correlation is observed. The absence of a trend suggests that variability in prey movement, clutter, and localisation uncertainty masks or overrides the predicted coupling in natural foraging settings, allowing bats to adapt call duration and interpulse interval more independently than the model prescribes.

The behavioural profiles show that the responsivity framework reproduces the dominant empirical trends (panels a–d) and predicts specific parameter couplings (panels e–f), revealing where natural behaviour deviates from the idealised model. The discrepancy in panels (e) and (f) underscores the influence of measurement constraints and environmental complexity in the field, while the convergence in panels (a–d) highlights the robustness of the framework in capturing the primary structure of echolocation behaviour.

4.6 Empirical Evidence for Reaction Time Limits

Studies on natural echolocation behaviour have rarely directly quantified the temporal limits of sensory-motor reactions in echolocating bats. The prey removal experiments by Geberl et. al, 2015 [6] provide a rare and highly relevant dataset. In their study, prey items were removed during the final buzz phase of *Myotis daubentonii*, at time points ranging from 3 to 240 ms before expected capture. The bats responded flexibly: when prey was removed more than ∼150 ms before contact, buzz was often shortened or omitted, whereas removals closer to contact elicited nearly complete buzz sequences despite the absence of prey. Acoustic reaction times were estimated at 80–90 ms, while motor reactions such as aborting capture behaviour lagged by a similar interval. Importantly, very late removals (<20 ms before interception) did not alter the vocal sequence, indicating a point of no return in the control loop.

These findings map directly onto predictions of the responsivity framework. In our simulations, buzz readiness was reached before buzz onset for moderate velocities ($v \approx 2$–3 m/s, $k_r \approx 4$–5), and the available reaction window T_{b^*} narrowed to 4–6 ms at high responsivity (Figures 5a, 5b). Thus, the empirical range of prey-removal outcomes in *M. daubentonii* corresponds well to the predicted spatio-temporal dynamics: removals occurring earlier than T_{b^*} elicit adaptive responses (buzz shortening or abandonment), while perturbations occurring inside the minimal window remain undetected, consistent with the observed continuation of complete buzz sequences.

Geberl et al. [6] speculated that the failure to adapt when prey was removed ∼3 ms before contact reflected a *point of no return*. Within our framework, this point corresponds precisely to the theoretical reaction limit T_{b^*}—the fastest temporal adaptation achievable by the sonar control loop. Therefore, the agreement between simulations and empirical observations lends strong support to the interpretation of T_{b^*} as a hard biophysical bound on sensorimotor reactivity.

To date, the experiments of Geberl et al. [6] remain the only field-based manipulation that directly probes the reaction time window in echolocating bats. Their results and our predictive derivations underscore the value of the responsivity framework as a mechanistic tool.

4.7 Predictive Mechanism and Behavioural Interpretation

Although the framework is theoretically presented, its strength lies in providing a predictive mechanism for interpreting echolocation behaviour from simple call recordings. Because the equations are grounded in biophysical constraints, they allow a large set of parameters to be recovered without direct spatial tracking.

The hyperbolic relation between call rate and distance (equation 19) enables instantaneous range estimation purely from timing data (Figure 4II). Differentiation of this relation yields a direct estimator of relative velocity (equation 24), showing how dynamic changes in call rate reflect approach speed (Figure 4.I&IV). Similarly, the definition of responsivity (equation 6) predicts the inflexion point of maximal temporal sensitivity, providing an objective criterion for identifying buzz readiness (Figure 2). This prediction naturally extends to duration control: the contraction of call duration emerges when the echo delay and minimal reaction window jointly constrain the processing interval (Figure 1d).

These relations show how the framework offers a compact predictive model. From a simple sequence of calls, one can reconstruct distance to target, approximate velocity, identify the onset of buzz readiness, and interpret call duration adjustments. This predictive capability makes the framework a retrospective descriptive tool and a prospective analytical method that bridges measurable acoustics with the underlying dynamics of sensorimotor control.

4.8 Generalisability Across Echolocation Modes

The framework presented in this study implicitly assumes that sensory processing occurs after the complete return of the emitted signal, i.e., that the full echo envelope is required for extracting the information necessary for adaptive control. This assumption holds naturally for frequency–modulated (FM) call emitters, where emission and reception are temporally segregated. However, in bats producing long or continuous call types—such as constant–frequency (CF), CF–FM, or quasi–CF (qCF) calls—where call–echo overlap is both unavoidable and well established [12, 37–39], the direct application of the present parameters requires reconsideration.

While a detailed extension of the model is beyond the current scope, several lines of evidence suggest that the responsivity principle may still hold under modified assumptions. CF bats are known to adjust their call duration with range [38, 40, 41], and numerous studies indicate that their information processing occurs predominantly in the spectral domain. Hybrid call types often include an FM tail, which dominates during prey interception in species such as *Noctilio leporinus* and *N. albiventris* [42–45], and is speculated to play a role in obstacle avoidance in *Rhinolophus sp* [41]. Moreover, neurophysiological studies in CF–FM species such as *Pteronotus* spp. reveal neural correlates for both FM and CF processing pathways [22, 46–48]. Together, these findings imply that CF systems may implement an analogous responsivity principle, but one in which the relevant feedback signal is spectrally rather than temporally defined.

A minimal extension of the model could thus relax the assumption of complete echo reception and instead evaluate the point of sufficient information–i.e., the earliest moment at which the echo contains enough spectral content to guide the following adaptive action. This perspective also clarifies why bats shorten call duration with decreasing range: if full echo reception were strictly required, such adaptations would be maladaptive. Instead, redundancy in long CF calls may serve other functions, while the onset of sufficient spectral feedback provides a viable

temporal anchor for responsivity-based regulation.

Future work will explore these considerations to extend the framework to continuous and hybrid sonar systems.

5 CONCLUSION

The responsivity framework unites the acoustic, kinematic, and neurophysiological dimensions of bat echolocation within a single predictive model. Formalising the temporal scaling between echo delay, call rate, and reaction time transforms simple call sequences into a source of rich quantitative inference, allowing estimation of distance, velocity, and behavioural thresholds without direct spatial tracking. The agreement between simulations, analytical derivations, and field data demonstrates that the framework captures the emergent structure of sonar behaviour and defines its biophysical boundaries.

However, establishing the model parameters as physiological ground truths will require further validation—both through dedicated experiments designed to measure the neural and behavioural correlates of responsivity, and through retrospective analyses of existing datasets that can be reinterpreted under this framework. In a broader sense, the model reveals how adaptive control in biological systems is constrained by the pace of feedback itself—an insight extending beyond bat biosonar to general principles of sensory–motor coordination in time-limited environments.

6 DECLARATIONS

Ethics approval and consent to participate

Not applicable. This study did not involve experiments on animals or humans.

Consent for publication

Not applicable.

Availability of data and materials

The following digital resources have been made available in support of the research presented in this work.

1. **Analytical software tools for applying the methods of the responsivity framework:**
   Code archived at Zenodo DOI: `https://doi.org/10.5281/zenodo.15801315`.
   The corresponding GitHub repository is available at: `https://github.com/raviumadi/analyse_responsivity`.

2. **The comprehensive field data set with analytical scripts:**
   Archieved at Zenodo DOI: `https://doi.org/10.5281/zenodo.15854830`
   Also see the corresponding GitHub repository at: `https://github.com/raviumadi/biosonar_responsivity`

3. ***Vespertillio numeralis* The simulated echolocation code is included in the repo listed above.**

Competing Interests

The author(s) declare no competing interests.

Funding

A part of the DFG Grant WI1518/18-1 supported the funding for the field study.

Author contributions

RU: Conceptualisation, Methodology, Software, Validation, Formal Analysis, Investigation, Data Curation, Writing – Original Draft, Visualisation, Project Administration.
UF: Supervision, Validation, Resources, Writing – Review & Editing, Funding Acquisition.

Acknowledgements

We extend our gratitude to our colleagues at the Technical University of Munich (TUM) for their valuable discussions and constructive feedback throughout the course of this work. We thank Christian Fink for his technical assistance in constructing the field array. We also thank the anonymous reviewer(s) for their insightful critique, which helped refine and strengthen the manuscript's narrative and conceptual depth.

Author's Note

We fondly refer to the simulated bat as *Vespertillio numeralis* – species native to the domain of simulation.

REFERENCES

1. Griffin, D. R. & Galambos, R. The Sensory Basis of Obstacle Avoidance by Flying Bats. *Journal of Experimental Zoology* **86,** 481–506. ISSN: 1097-010X. https://onlinelibrary.wiley.com/doi/abs/10.1002/jez.1400860310 (2022) (1941).
2. Griffin, D. R., Webster, F. A. & Michael, C. R. The Echolocation of Flying Insects by Bats. *Animal Behaviour* **8,** 141–154. ISSN: 0003-3472. https://www.sciencedirect.com/science/article/pii/0003347260900221 (2022) (July 1, 1960).
3. Griffin, D. R. How Bats Guide Their Flight by Supersonic Echoes. *American Journal of Physics* **12,** 342–345. ISSN: 0002-9505. https://aapt.scitation.org/doi/10.1119/1.1990634 (2022) (Dec. 1944).
4. Griffin, D. R. Return to the Magic Well: Echolocation Behavior of Bats and Responses of Insect Prey. *BioScience* **51,** 555–556. ISSN: 0006-3568. https://doi.org/10.1641/0006-3568(2001)051[0555:RTTMWE]2.0.CO;2 (2024) (July 1, 2001).
5. Moss, C. F. & Surlykke, A. Auditory Scene Analysis by Echolocation in Bats. *The Journal of the Acoustical Society of America* **110,** 2207–2226. ISSN: 0001-4966. PMID: 11681397 (2001).
6. Geberl, C., Brinkløv, S., Wiegrebe, L. & Surlykke, A. Fast Sensory–Motor Reactions in Echolocating Bats to Sudden Changes during the Final Buzz and Prey Intercept. *Proceedings of the National Academy of Sciences* **112,** 4122–4127. https://www.pnas.org/doi/full/10.1073/pnas.1424457112 (2024) (Mar. 31, 2015).
7. Wohlgemuth, M. & Moss, C. Active Listening in a Complex Environment. *Proceedings of Meetings on Acoustics* **19,** 010030. ISSN: 1939-800X. https://doi.org/10.1121/1.4800959 (2025) (May 14, 2013).
8. Moss, C. F. & Surlykke, A. Probing the Natural Scene by Echolocation in Bats. *Frontiers in Behavioral Neuroscience* **4.** ISSN: 1662-5153. https://www.frontiersin.orghttps://www.frontiersin.org/journals/behavioral-neuroscience/articles/10.3389/fnbeh.2010.00033/full (2025) (Aug. 5, 2010).
9. Jakobsen, L. & Surlykke, A. Vespertilionid Bats Control the Width of Their Biosonar Sound Beam Dynamically during Prey Pursuit. *Proceedings of the National Academy of Sciences* **107,** 13930–13935. ISSN: 0027-8424. PMID: 20643943 (2010).
10. Wilson, A. M. *et al.* Locomotion Dynamics of Hunting in Wild Cheetahs. *Nature* **498,** 185–189. ISSN: 1476-4687. https://www.nature.com/articles/nature12295 (2025) (June 2013).
11. Perrine, J. O. The Doppler and Echo Doppler Effect. *American Journal of Physics* **12,** 23–28. ISSN: 0002-9505, 1943-2909. http://aapt.scitation.org/doi/10.1119/1.1990527 (2022) (Feb. 1944).
12. Trappe, M. & Schnitzler, H. .-. Doppler-Shift Compensation in Insect-Catching Horseshoe Bats. *Naturwissenschaften* **69,** 193–194. ISSN: 0028-1042, 1432-1904. http://link.springer.com/10.1007/BF00364902 (2023) (Apr. 1982).
13. Bell, G. P. & Fenton, M. B. The Use of Doppler-shifted Echoes as a Flutter Detection and Clutter Rejection System: The Echolocation and Feeding Behavior of Hipposideros Tuber (Chiroptera :Hipposideridae). *Behav Ecol Sociobiol,* 109–114 (1984).
14. Schoeppler, D., Kost, K., Schnitzler, H.-U. & Denzinger, A. Transmitter and Receiver of the Low Frequency Horseshoe Bat Rhinolophus Paradoxolophus Are Functionally Matched for Fluttering Target Detection. *Journal of Comparative Physiology. A, Neuroethology, Sensory, Neural, and Behavioral Physiology* **209,** 191–202. ISSN: 0340-7594. PMID: 36136120. https://www.ncbi.nlm.nih.gov/pmc/articles/PMC9898408/ (2025) (2023).
15. Yoshida, S., Hase, K., Heim, O., Kobayasi, K. I. & Hiryu, S. Doppler Detection Triggers Instantaneous Escape Behavior in Scanning Bats. *iScience,* 109222. ISSN: 25890042. https://linkinghub.elsevier.com/retrieve/pii/S2589004224004437 (2024) (Feb. 2024).

16. Jakobsen, L. *et al.* Velocity as an Overlooked Driver in the Echolocation Behavior of Aerial Hawking Vespertilionid Bats. *Current Biology,* S096098222401710X. ISSN: 09609822. https://linkinghub.elsevier.com/retrieve/pii/S096098222401710X (2025) (Jan. 2025).

17. Todorov, E. & Jordan, M. I. Optimal Feedback Control as a Theory of Motor Coordination. *Nature Neuroscience* **5,** 1226–1235. ISSN: 1097-6256, 1546-1726. https://www.nature.com/articles/nn963 (2025) (Nov. 2002).

18. Todorov, E. & Jordan, M. I. A Minimal Intervention Principle for Coordinated Movement. *Advances in Neural Information Processing Systems,* 27–34 (2003).

19. Umadi, R. Widefield Acoustics Heuristic: Advancing Microphone Array Design for Accurate Spatial Tracking of Echolocating Bats. *BMC Ecology and Evolution* **25,** 92. ISSN: 2730-7182. https://doi.org/10.1186/s12862-025-02441-4 (2025) (Sept. 8, 2025).

20. Umadi, R. *Array WAH: Microphone Array Design Tool* version V1.1.0. Zenodo, Aug. 2025. https://zenodo.org/records/16922627 (2025).

21. Ester, M., Kriegel, H.-P., Sander, J. & Xu, X. A Density-Based Algorithm for Discovering Clusters in Large Spatial Databases with Noise. *Proceedings of 2nd International Conference on Knowledge Discovery and Data Mining* **(KDD-96).**

22. Suga, N. & Horikawa, J. Multiple Time Axes for Representation of Echo Delays in the Auditory Cortex of the Mustached Bat. *Journal of Neurophysiology* **55,** 776–805. ISSN: 0022-3077, 1522-1598. https://www.physiology.org/doi/10.1152/jn.1986.55.4.776 (2025) (Apr. 1, 1986).

23. Wong, D., Maekawa, M. & Tanaka, H. The Effect of Pulse Repetition Rate on the Delay Sensitivity of Neurons in the Auditory Cortex of the FM Bat, Myotis Lucifugus. *Journal of Comparative Physiology A* **170.** ISSN: 0340-7594, 1432-1351. http://link.springer.com/10.1007/BF00191456 (2025) (Apr. 1992).

24. Suga, N., O'Neill, W. E., Kujirai, K. & Manabe, T. Specificity of Combination-Sensitive Neurons for Processing of Complex Biosonar Signals in Auditory Cortex of the Mustached Bat. *Journal of Neurophysiology* **49,** 1573–1626. ISSN: 0022-3077, 1522-1598. https://www.physiology.org/doi/10.1152/jn.1983.49.6.1573 (2025) (June 1, 1983).

25. Bartenstein, S. K., Gerstenberg, N., Vanderelst, D., Peremans, H. & Firzlaff, U. Echo-Acoustic Flow Dynamically Modifies the Cortical Map of Target Range in Bats. *Nature Communications* **5,** 4668. ISSN: 2041-1723. https://www.nature.com/articles/ncomms5668 (2025) (Aug. 18, 2014).

26. Dear, S. P., Simmons, J. A. & Fritz, J. A Possible Neuronal Basis for Representation of Acoustic Scenes in Auditory Cortex of the Big Brown Bat. *Nature* **364** (Aug. 1993).

27. Gallivan, J. P., Chapman, C. S., Wolpert, D. M. & Flanagan, J. R. Decision-Making in Sensorimotor Control. *Nature Reviews Neuroscience* **19,** 519–534. ISSN: 1471-003X, 1471-0048. https://www.nature.com/articles/s41583-018-0045-9 (2025) (Sept. 2018).

28. Todorov, E. Optimality Principles in Sensorimotor Control. *Nature Neuroscience* **7,** 907–915. ISSN: 1097-6256, 1546-1726. https://www.nature.com/articles/nn1309 (2025) (Sept. 2004).

29. Scott, S. H. Optimal Feedback Control and the Neural Basis of Volitional Motor Control. *Nature Reviews Neuroscience* **5,** 532–545. ISSN: 1471-003X, 1471-0048. https://www.nature.com/articles/nrn1427 (2025) (July 2004).

30. Utkin, V. Sliding Mode Control Design Principles and Applications to Electric Drives. *IEEE Transactions on Industrial Electronics* **40,** 23–36. ISSN: 1557-9948. https://ieeexplore.ieee.org/document/184818 (2025) (Feb. 1993).

31. Edwards, C. & Spurgeon, S. K. *Sliding Mode Control: Theory And Applications* 237 pp. ISBN: 978-0-429-07593-3 (CRC Press, London, Aug. 27, 1998).

32. Zeinali, M. & Notash, L. Adaptive Sliding Mode Control with Uncertainty Estimator for Robot Manipulators. *Mechanism and Machine Theory* **45,** 80–90. ISSN: 0094-114X. https://www.sciencedirect.com/science/article/pii/S0094114X09001530 (2025) (Jan. 1, 2010).

33. Pruszynski, J. A. & Scott, S. H. Optimal Feedback Control and the Long-Latency Stretch Response. *Experimental Brain Research* **218,** 341–359. ISSN: 1432-1106. https://doi.org/10.1007/s00221-012-3041-8 (2025) (May 1, 2012).

34. Harris, C. M. & Wolpert, D. M. Signal-Dependent Noise Determines Motor Planning. *Nature* **394,** 780–784. ISSN: 1476-4687. https://www.nature.com/articles/29528 (2025) (Aug. 1998).

35. Moss, C. F., Bohn, K., Gilkenson, H. & Surlykke, A. Active Listening for Spatial Orientation in a Complex Auditory Scene. *PLOS Biology* **4,** e79. ISSN: 1545-7885. https://journals.plos.org/plosbiology/article?id=10.1371/journal.pbio.0040079 (2025) (Mar. 7, 2006).

36. Hulgard, K. & Ratcliffe, J. M. Sonar Sound Groups and Increased Terminal Buzz Duration Reflect Task Complexity in Hunting Bats. *Scientific Reports* **6,** 21500. ISSN: 2045-2322. https://www.nature.com/articles/srep21500 (2025) (Feb. 9, 2016).

37. Schuller, G. The Role of Overlap of Echo with Outgoing Echolocation Sound in the Bat Rhinolophus Ferrumequinum. *Naturwissenschaften* **61,** 171–172. ISSN: 1432-1904. https://doi.org/10.1007/BF00602598 (2022) (Apr. 1, 1974).

38. Schnitzler, H.-U., Hackbarth, H., Heilmann, U. & Herbert, H. Echolocation Behavior of Rufous Horseshoe Bats Hunting for Insects in the Flycatcher-Style. *Journal of Comparative Physiology A* **157,** 39–46. ISSN: 0340-7594, 1432-1351. http://link.springer.com/10.1007/BF00611093 (2025) (1985).

39. Fenton, M. B., Faure, P. A. & Ratcliffe, J. M. Evolution of High Duty Cycle Echolocation in Bats. *Journal of Experimental Biology* **215,** 2935–2944. ISSN: 1477-9145, 0022-0949. https://journals.biologists.com/jeb/article/215/17/2935/10996/Evolution-of-high-duty-cycle-echolocation-in-bats (2022) (Sept. 1, 2012).

40. Jen, P. H. S. & Kamada, T. Analysis of Orientation Signals Emitted by the CF-FM Bat,Pteronotus p. Parnellii and the FM Bat,Eptesicus Fuscus during Avoidance of Moving and Stationary Obstacles. *Journal of Comparative Physiology - A* **148,** 389–398. ISSN: 0340-7594, 1432-1351. http://link.springer.com/10.1007/BF00679023 (2025) (1982).

41. Vogler, B. & Neuweiler, G. Echolocation in the Noctule (Nyctalus Noctula) and Horseshoe Bat (Rhinolophus Ferrumequinum). *Journal of Comparative Physiology - A* **152,** 421–432. ISSN: 0340-7594, 1432-1351. http://link.springer.com/10.1007/BF00606247 (2025) (1983).

42. Suthers, R. A. Acoustic Orientation by Fish-Catching Bats. *Journal of Experimental Zoology* **158,** 319–347. ISSN: 1097-010X. https://onlinelibrary.wiley.com/doi/abs/10.1002/jez.1401580307 (2025) (1965).

43. Suthers, R. A. & Fattu, J. M. Fishing Behaviour and Acoustic Orientation by the Bat (Noctilio Labialis). *Animal Behaviour* **21,** 61–66. ISSN: 00033472. https://linkinghub.elsevier.com/retrieve/pii/S0003347273800405 (2025) (Feb. 1973).

44. Hartley, D. J., Campbell, K. A. & Suthers, R. A. The Acoustic Behavior of the Fish-catching Bat, Noctilio Leporinus, during Prey Capture. *The Journal of the Acoustical Society of America* **86,** 8–27. ISSN: 0001-4966, 1520-8524. https://pubs.aip.org/jasa/article/86/1/8/633178/The-acoustic-behavior-of-the-fish-catching-bat (2025) (July 1, 1989).

45. Schnitzler, H.-U., Kalko, E. K. V., Kaipf, I. & Grinnell, A. D. Fishing and Echolocation Behavior of the Greater Bulldog Bat, Noctilio Leporinus, in the Field. *Behavioral Ecology and Sociobiology* **35,** 327–345. ISSN: 0340-5443, 1432-0762. http://link.springer.com/10.1007/BF00184422 (2025) (Nov. 1994).

46. Yan, J. & Suga, N. Corticofugal Modulation of Time-Domain Processing of Biosonar Information in Bats. *Science* **273,** 1100–1103. ISSN: 0036-8075, 1095-9203. https://www.science.org/doi/10.1126/science.273.5278.1100 (2025) (Aug. 23, 1996).

47. Ma, X. & Suga, N. Corticofugal Modulation of Duration-Tuned Neurons in the Midbrain Auditory Nucleus in Bats. *Proceedings of the National Academy of Sciences* **98,** 14060–14065. https://www.pnas.org/doi/10.1073/pnas.241517098 (2025) (Nov. 20, 2001).

48. Suzuki, M. & Suga, N. Acuity in Ranging Based on Delay-Tuned Combination-Sensitive Neurons in the Auditory Cortex of Mustached Bats. *Hearing Research* **350,** 189–204. ISSN: 0378-5955. https://www.sciencedirect.com/science/article/pii/S0378595516305998 (2025) (July 1, 2017).